

Article

# Exiting Inflation with a Smooth Scale Factor

Harry Oslislo and Brett Altschul \* 

Department of Physics and Astronomy, University of South Carolina, Columbia, SC 29208, USA

\* Correspondence: altschul@mailbox.sc.edu

**Abstract:** The expectation that the physical expansion of space occurs smoothly may be expressed mathematically as a requirement for continuity in the time derivative of the metric scale factor of the Friedmann–Robertson–Walker cosmology. We explore the consequences of imposing such a smoothness requirement, examining the forms of possible interpolating functions between the end of inflation and subsequent radiation- or matter-dominated eras, using a straightforward geometric model of the interpolating behavior. We quantify the magnitude of the cusp found in a direct transition from the end of slow-roll inflation to the subsequent era, analyze the validity of several smooth interpolator candidates, and investigate equation-of-state and thermodynamic constraints. We find an order-of-magnitude increase in the size of the universe at the end of the transition to a single-component radiation or matter era. We also evaluate the interpolating functions in terms of the standard theory of preheating and determine the effect on the number of bosons produced.

**Keywords:** early universe; inflation; preheating

## 1. Introduction

The problem of trying to reconcile physical theories regarding the form and evolution of the primordial universe with modern cosmological observations has occupied researchers for decades. Providing a complete explanation for the origins of the characteristics that the universe exhibits today has been challenging. We witness extreme uniformity and flatness and the absence of certain particles predicted in some Grand Unified Theory (GUT) models. Many physicists have detailed these well-known difficulties in texts and expository papers; see, for example, Refs. [1–9].

The issue of uniformity has the name the *horizon problem*. We see a homogeneous, isotropic universe on large scales. Despite the almost incomprehensible longevity of the universe, it is simply too immense to have grown to be uniform on large scales. Causality demands that local homogeneity takes time to develop, with equilibrium conditions dispersing at a rate no greater than the speed of light. Two local homogeneous elements dispersed in time must retain a causal connection to remain in equilibrium with one another. Yet opposite sides of the universe appear nearly identical to us. Even if we assume they started that way, not enough time has passed for space to have expanded a great enough distance to maintain the equilibrium—at least not according to the physics we understand—with signaling bounded by the limit of the speed of light. Cosmologists assess uniformity primarily using the temperature of the Cosmic Microwave Background (CMB), which is the thermal radiation emitted as the matter in the universe was cooling and transitioning from a conductive, opaque plasma to a neutral, transparent gas. The widely accepted standard is  $T_{\text{CMB}} \approx 2.7255 \text{ K}$  [10]. An early CMB probe, the Cosmic Background Explorer, found the temperature variation from this mean to be on the order of  $10^{-5} \text{ K}$ . Each causally connected portion of the CMB that should have been able to thermalize before the recombination photons began to stream freely along their paths toward the Earth covers a solid angle of approximately  $0.013 \text{ sr}$  in the sky, so that about  $10^4$  such solid angles make up the CMB. *How then, cosmologists ask, did 10,000 discrete portions of the CMB, which do not appear to have been causally connected at the time of recombination, collectively equilibrate at a*



**Citation:** Oslislo, H.; Altschul, B. Exiting Inflation with a Smooth Scale Factor. *Symmetry* **2023**, *15*, 2042. <https://doi.org/10.3390/sym15112042>

Academic Editors: Tomohiro Inagaki, Alberto Ruiz Jimeno and Olga Kodolova

Received: 10 October 2023  
Revised: 3 November 2023  
Accepted: 6 November 2023  
Published: 10 November 2023



**Copyright:** © 2023 by the authors. Licensee MDPI, Basel, Switzerland. This article is an open access article distributed under the terms and conditions of the Creative Commons Attribution (CC BY) license (<https://creativecommons.org/licenses/by/4.0/>).

common temperature that is uniform to within the order of  $10^{-5}$  K [1]? A period of superluminal expansion provided by inflation could provide the missing causal connection.

Expansion itself does not change the inherent topology of the universe: a universe that is closed, open, or flat remains so. However, expansion makes any curvature appear locally more flat. The Planck Collaboration has measured the spatial curvature  $\Omega_k$  as  $0.001 \pm 0.002$  [11], which means our nearly flat universe presents a second cosmological difficulty: the *flatness problem*. The scale factors  $a(t)$  of matter-dominated and radiation-dominated cosmologies are proportional to  $t^{2/3}$  and  $t^{1/2}$ , respectively. According to the first Friedman equation [1,12],  $\Omega_k$  scales as  $1/\dot{a}^2$ , so that in the absence of any other influences, the longevity of the universe means that consistency with the Planck measurement requires that the curvature at the beginning of the radiation-dominated era must have been extraordinarily small. Again, inflation offers a remedy: the inflationary exponential scale factor would tend to drive down the spatial curvature to a level that could support subsequent evolution to the value observed today.

The additional *monopole problem* arises from the predictions of some GUT models [13,14], which predict that a phase transition breaks the symmetry between the strong and weak forces when the temperature of the universe drops to a level consistent with the energy scale  $10^{16}$  GeV. A result would be the formation of a dust of massive magnetic monopoles, with a density that is subsequently proportional to  $a^{-3}$ , potentially, thereby, blocking the radiation and matter eras from taking place [5]. The monopole problem calls for a mechanism to reconcile the GUT prediction of the creation of these massive particles with our accepted understanding of the chronology of the early universe and current cosmological observation. Inflation could provide dilution that would make magnetic monopoles so few and far apart that finding them would be essentially impossible.

### 1.1. The Inflation Solution

In his groundbreaking paper in 1981 [15], Alan Guth introduced inflation as a theory to address the inexplicable horizon, flatness, and monopole problems. However, he also acknowledged the difficulty his mechanism created: an exit from the false vacuum that drives inflation involved quantum tunneling from a false to the true vacuum state, an effect that would occur primarily in localized bubbles—that is, discrete regions subsequently characterized by the Klein–Gordon scalar field that drives inflation (the inflaton  $\phi$ ) having settled into its true vacuum state. Moreover, expansion of space would continue between the bubbles (where such tunneling had not yet occurred), and as a result, we would expect to see parcels of nonuniform space today. Intersecting bubbles would have similar effects. This model of inflation, thus, predicted a universe inconsistent with observation; Guth’s original theory lacks a *graceful exit*.

In 1982, inflation pioneer Andrei Linde sought to solve the graceful exit problem with a new theory: *slow-roll inflation* [16]. Instead of starting in a false vacuum, the inflaton rolls down a potential energy plateau to a minimum where it oscillates around a true vacuum state, which graph (a) of Figure 1 depicts schematically. The assumption that the potential energy of the inflaton dominates the kinetic energy for a sufficient time results in exponential inflation.

The *slow-roll* condition implies  $\ddot{\phi} \rightarrow 0$ , so that the equation of motion of the scalar field

$$\ddot{\phi} + 3H\dot{\phi} + V(\phi)_{,\phi} = 0, \quad (1)$$

reduces to

$$3H\dot{\phi} = -V(\phi)_{,\phi}. \quad (2)$$

The Hubble parameter  $H$  is the expansion rate of the universe,  $V(\phi)$  is the potential of the inflaton, and the comma denotes the partial derivative with respect to  $\phi$ . The theory

assumes that the magnitudes of both the density and pressure of the inflaton become approximately equal to the potential by treating the inflaton condensate as a perfect fluid:

$$\rho = \frac{1}{2}\dot{\phi}^2 + V(\phi) \approx V(\phi) \quad (3)$$

$$p = \frac{1}{2}\dot{\phi}^2 - V(\phi) \approx -V(\phi). \quad (4)$$

In this regime, the second Friedmann equation [1,12], commonly known as the *acceleration equation*, because it governs  $\ddot{a}$ , is essentially

$$\frac{\ddot{a}(t)}{a(t)} = -\frac{4\pi G}{3}(\rho + 3p) = \frac{8\pi G}{3}\rho. \quad (5)$$

In our notation,  $\hbar = 1$  and  $c = 1$  hereafter unless otherwise noted. Thus, the expansion of space undergoes inflationary acceleration,  $\frac{\ddot{a}}{a} > 0$ , as a result. The first Friedman equation,

$$H^2 + \frac{k}{a^2} = \frac{8\pi G}{3}\rho, \quad (6)$$

with  $H^2 = \left(\frac{\dot{a}}{a}\right)^2 \gg \frac{k}{a^2}$ , yields the scale factor solution

$$a(t) = a_0 e^{Ht}. \quad (7)$$

This is the exponential expansion of space predicted by the theory of slow-roll inflation [8,17]. A period of superluminal expansion would explain the homogeneity and isotropy of the observable universe by providing the necessary causal connection to solve the horizon problem. Superluminal expansion would also flatten the spatial curvature and decrease the density of magnetic monopoles. Numerical analysis provides insight into the question of the number of  $e$ -folds of expansion necessary to resolve these problems. However, this solution comes with its own associated shortcoming: producing an outcome consistent with modern observations demands very specific initial conditions.

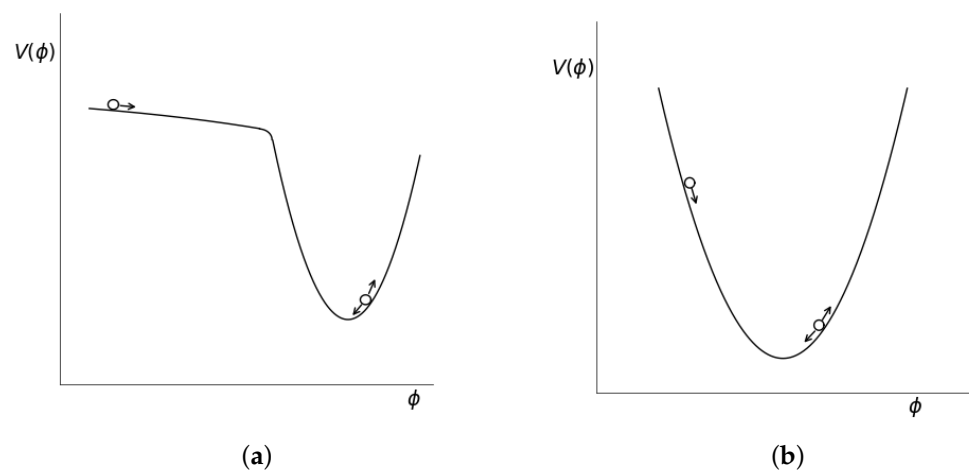


**Figure 1.** The contrast between the potentials of slow-roll inflation, shown in (a), and chaotic inflation, shown in (b). Slow-roll inflation requires a plateau to generate enough  $e$ -folds of inflationary expansion to solve the horizon, flatness, and monopole problems. In chaotic inflation, the effects of the friction term in the equation of motion replace that of the plateau in keeping the inflaton from moving to the true vacuum too quickly. After inflation, both models involve the inflaton oscillating around a minimum potential during a period of reheating, which we review in Section 1.2.

Although the underlying physics of inflation (such as the existence of the inflaton field) remains unsubstantiated experimentally, the framework of inflation is widely accepted

among cosmologists as a way of providing an underlying solution to various cosmological problems. Over the years, researchers have revised the concept by devising a diverse body of new theories. For our purposes, we shall focus on Linde's solution to the problem of the requirement of specific initial conditions in the slow-roll theory. In 1983, he published his theory of *chaotic inflation* [18]. See Ref. [19] for a recent overview of the theory. In its simplest version [17], the inflaton potential has the form  $V(\phi) = \frac{1}{2}m^2\phi^2$ . The plateau is absent, and in an expanding universe, the friction term  $3H\dot{\phi}$  in the inflaton equation of motion (1) has the effect of restricting the motion of the inflaton, as the slow roll plateau does, resulting again in exponential expansion. Figure 1 shows the two contrasting potentials.

Cosmologists have applied a variety of approaches to estimating the amount of inflation necessary to solve the horizon, flatness, and monopole problems. The amount by which the cosmos expands is normally expressed in terms of the number of times the size has increased by a constant factor—in other words, the number of the  $e$ -folds (or nepers)  $N = \log \frac{a(t_f)}{a(t_i)}$ . Linde [17] reports that a quadratic inflaton potential creates a wavelength for the inflaton comparable in size to our observable universe after about 61  $e$ -folds. In a detailed analysis, Lyth [20] finds that, for a quartic inflaton potential, a range of  $e$ -fold values from 47 to 61 results in a universe on the present scale. He further explains that at a minimum, more than 14  $e$ -folds are needed to generate perturbations leading to structure formation, and that an extended period of domination of the inflaton kinetic term could increase his estimates of  $N$  by nearly 14; therefore, he concludes with an estimate of  $14 < N < 75$ .

Other researchers have performed analyses to determine the number of  $e$ -folds required to solve specific inflationary problems [21]. Solving the horizon problem entails that the comoving Hubble radius at the beginning of inflation  $[a(t_i)H(t_i)]^{-1}$  must contain what has become the comoving Hubble radius today  $[a(t_0)H(t_0)]^{-1}$ , so that the comoving  $[a(t_0)H(t_0)]^{-1}$  could have thermalized before expanding through the postinflationary epochs of the universe up to the present. The Hubble radius is the distance light travels in time  $t = H^{-1}$ . Thus, we have

$$[a(t_i)H(t_i)]^{-1} \geq [a(t_0)H(t_0)]^{-1} \quad (8)$$

$$\frac{1}{H(t_i)} \geq \frac{1}{H(t_0)} \frac{a(t_i)}{a(t_0)} = \frac{1}{H(t_0)} \frac{a(t_f)}{a(t_0)} \frac{a(t_i)}{a(t_f)} = \frac{1}{H(t_0)} \frac{a(t_f)}{a(t_0)} e^{-N} \quad (9)$$

$$-N \leq \log \left[ \frac{H(t_0)}{H(t_i)} \frac{a(t_0)}{a(t_f)} \right] = \log \left[ \frac{H(t_0)}{H(t_i)} \frac{T(t_f)}{T(t_0)} \right] = \log \left[ \frac{H(t_0)}{T(t_0)} \frac{T(t_f)}{H(t_i)} \right]. \quad (10)$$

In Equation (10) we use the inverse relation between the scale factor and temperature, which is derived in Appendix A for reference. Parameter values  $T(t_0) \approx 2.75$  K and  $H(t_0) \approx 100$  km/s/Mpc lead to

$$N \geq 67 + \log \left[ \frac{H(t_i)}{T(t_f)} \right], \quad (11)$$

which indicates that  $N$  is at least 67, because the temperature  $H(t_i)$  represents is greater than  $T(t_f)$ .

### 1.2. Reheating

The expansion of space by inflation dilutes the number densities of all particles and leaves the universe cold, with energy concentrated primarily in the inflaton. Following the end of inflation, reheating results in the transfer of energy from the inflaton to standard model particles or their precursors. Reheating has two stages: first, the transfer of energy, and then the subsequent thermalization to a temperature sufficient to promote nucleosynthesis of light elements. A mechanism developed by Lev Kofman, Andrei Linde, and Alexei Starobinsky in their iconic 1997 paper, "Towards the Theory of Reheating after

Inflation” [22], which they call *preheating* because it precedes thermalization, supersedes earlier explanations of reheating by way of perturbation theory and narrow parametric resonance. We reference a selection of the wide range of literature available on the subject of preheating [7,23–26].

A preheating framework appears to be necessary, because perturbative processes prove too slow and inefficient to raise the reheating temperature enough to support nucleosynthesis. Also, the perturbative approach required certain conditions and treated inflatons collectively in a state of superposition of individual particles, each capable of decaying independently—rather than as coherent semiclassical fields. On the other hand, narrow parametric resonance models followed the approach that the inflatons formed a homogeneous, coherent, oscillating wave appropriate for classical treatment. In narrow parametric resonance, an inflaton wave interacts as a background source for a second scalar field  $\chi$ . However, this theory itself can be problematic. Because the modes of the scalar field  $\chi$  have physical wavelengths, the expansion of space redshifts modes outside the borders of the resonance band and also makes the band more narrow. In addition, the expansion and the decay of the inflaton into  $\chi$  particles decrease the amplitude of the coherent inflaton wave. The number of particles being produced instantaneously is proportional to both the number of  $\chi$  particles previously created and to the inflaton amplitude, so that the effects of expansion and decay lower the efficiency of the resonant conversion and tend to suppress the growth of the  $\chi$  population. Narrow parametric resonance, thus, typically terminates well before reheating is complete.

The parametric resonance in preheating models is instead broad: all modes less than a specific momentum participate in the  $\phi$ - $\chi$  coupling. A nonadiabatic transfer of energy leads to exponential growth in the number and number density of the  $\chi$  quanta. Moreover, the expansion of space can actually make the resonance more effective by gradually redshifting additional modes down to below the maximum momentum, making them part of the process. The end of reheating depends on the possible range of values of parameters involved in preheating and the complex dynamics of backreaction and rescattering. However, preheating may still not be sufficient to complete reheating, and the reheating process may have to revert to a period of narrow parametric resonance, perturbative decay, or both to arrive at a temperature that is suitable for thermalization but not high enough to produce very massive particles like monopoles.

In Section 2, the reader will find a description of the cusp discontinuity inherent in inflationary theories involving an exponential scale factor and our approach to quantifying the extent of the cusp. Section 3 introduces a method for finding an interpolating function to replace the cusp, by detailing the geometry of a simple circular model. Then, in Section 4, we focus on finding a more realistic interpolating function. We derive the formalism establishing smoothness in the expansion of space at the end of inflation and analyze the implications of the most straightforward interpolating candidates: power-law functions. The equation-of-state and thermodynamic constraints provide additional means of restricting possible interpolating functions, and this is discussed in Section 5. We analyze the effect on the size of the universe of a horizontal parabola-like power law serving as a transitional interpolating function in Section 6. Finally, we look at further numerical analyses to determine the effect on the scalar  $\chi$  number and number density predicted by the Kofman, Linde, and Starobinsky (KLS) model of preheating in Section 7.

## 2. Period Scale Factors

The well-known expressions for the scale factor in the early universe include a curious unphysical approximation: a lack of smoothness at the end of the inflationary epoch. The inflationary and radiation-dominated scale factors,  $a_1(t)$  and  $a_2(t)$ , respectively, follow [1]

$$a_1(t) = a(t_i)e^{H(t-t_i)} \quad (12)$$

$$a_2(t) = a(t_f) \left( \frac{t}{t_f} \right)^{1/2}. \quad (13)$$

To demonstrate the discontinuity in  $\dot{a}$ , we assume contrariwise that the time derivatives of the scale factors are equal at the end of inflation,  $t_f$ :

$$\left. \frac{d}{dt} a_1(t) \right|_{t_f} = a(t_i) H e^{H(t-t_i)} \Big|_{t_f} = a(t_f) H \quad (14)$$

$$\left. \frac{d}{dt} a_2(t) \right|_{t_f} = \frac{a(t_f)}{\sqrt{t_f}} \frac{1}{2t_f^{1/2}} \Big|_{t_f} = \frac{a(t_f)}{2t_f}. \quad (15)$$

By first expressing the Hubble parameter  $H$  in terms of  $N$ , the number of inflationary  $e$ -folds of expansion, and then equating derivatives, we find

$$H = \frac{N}{t_f - t_i} \quad (16)$$

$$N = \frac{t_f - t_i}{2t_f} = \frac{1}{2} - \frac{t_i}{2t_f}. \quad (17)$$

Continuity of the derivatives requires that  $N \leq \frac{1}{2}$ , or else the time at the beginning of inflation is less than zero. Although much research into inflation has produced a wide range of proposed values for  $N$ , this result is particularly problematic. If taken literally, it would eliminate inflation as a solution to the kinds of problems the theory was designed to solve.

The primary goal of this work is to understand how a more model without a kink could affect the subsequent cosmology. In principle, a complete tracking of the equation-of-state parameters at and immediately after the end of inflation would seem to provide everything necessary to answer this question; however, to do this properly would require a full accounting of all the physics of the inflaton field whose false vacuum energy density drove the inflationary expansion. To study the transition at the end of inflation in a way that is relatively independent of the detailed collective dynamics of the inflaton, we adopt an phenomenological approach, looking at classes of mathematically reasonable interpolation functions for the scale factor  $a(t)$  itself, rather than the equation of state. On sufficiently short time scales, quantum and thermal fluctuations will mean that the equation of state of the cosmos does not actually need to have a quasi-equilibrium form, and any use of an analytical equation of state is necessarily an approximation. However, we shall continue with the conventional approach of considering a model with an approximate quasi-equilibrium equation of state, superposed on top of which there can be additional fluctuations in some of the degrees of freedom. The use of a single-component equation of state for the later postinflation epoch is naturally also an approximation; even in thermal equilibrium, the true equation of state will always receive contributions from all the quantum fields present in the theory—whether relativistic (radiation-like) or nonrelativistic (matter-like). However, the question of how many components of the energy-momentum content need to be taken into account to achieve full quantitative accuracy is separate from the issue of whether a thermodynamically descriptive equation of state exists at all. Even during a phase transition, there can be an interpolating equation of state (whose degree of smoothness is determined by the order of the transition). It is conceivable that a first-order phase transition may be so abrupt that the collective, thermodynamic description of the physics breaks down during the immediate transition period; and if this is how the universe behaves at the termination of inflation, then that would actually be a very interesting observation. However, that lies beyond the scope of this paper; indeed, this

work is specifically limited to the consideration of the opposite regime, in which the end of inflation is represented by a higher-order transition, and the physics of the immediately postinflationary era can be consistently described via a smoothly varying, continuous dynamical picture.

Our approach is complementary to the one adopted in Ref. [27], which worked to trace the effective value of parameter  $w$  (for the equation of state  $p = w\rho$ ) during the slightly later periods of preheating and reheating. That paper's authors noted the challenges of trying to specify the  $w$  parameter precisely; instead, they analyzed the parameter's time evolution and sought to find a suitably averaged value through lattice simulation. Their analysis concentrated on the evolution due to postinflation backreaction, which our analysis precedes. However, as part of their study, they by necessity included an estimate of the number of  $e$ -folds of additional expansion brought about by the coherent oscillations of the inflaton before backreaction. They estimated the number of  $e$ -folds to be approximately 3.07 for a quadratic inflaton potential, without regard to the form of the scale factor. In this work, we shall find that using a smooth scale factor similarly increases the expansionary effect by approximately 2 to 3  $e$ -folds, so that the two approaches are not in conflict.

### 2.1. Quantifying the Discontinuity

Although early universe estimates are themselves quite problematic because of the uncertainty in the values of basic parameters, using reasonable values can provide some insight into the mathematical relationship between the scale factors in different periods of cosmological evolution. We can estimate a value for  $a(t_f)$  by taking advantage of the inverse relation between the scale factor and temperature, in conjunction with estimates of temperature then and now,  $T(t_f)$  and  $T(t_0)$ , respectively,

$$a(t_f) = \frac{T(t_0)}{T(t_f)} \approx \frac{2.73 \text{ K}}{1.16 \times 10^{29} \text{ K}} \approx 10^{-29}, \quad (18)$$

since, by convention,  $a(t_0) = 1$ . The temperature of the CMB today is  $T(t_0) \approx 2.73 \text{ K}$  [10], and  $T(t_f)$  corresponds to the temperature equivalent to the value of  $H$  for a universe that supports the standard model, which is  $H \approx 10^{16} \text{ GeV}$  [28].

Next, we compare slopes at the end of inflation. The inflationary slope is

$$\dot{a}_1(t_f) \approx 10^{-13} \text{ GeV} \approx 10^{11} \text{ s}^{-1}. \quad (19)$$

For the radiation-era derivative, after solving Equation (16) for  $t_f$  and substituting it into Equation (15), we have

$$\dot{a}_2(t_f) = \frac{a(t_f)H}{2(N + Ht_i)} = \frac{\dot{a}_1(t_f)}{2(N + Ht_i)}. \quad (20)$$

The estimate by Liddle and Lyth that inflation began at  $t_i = 10^{-42} \text{ s}$  [2] leads to  $Ht_i \approx 0.02$ . A reasonable assumption is that  $N \approx 60$  [17,20,21], which results in a measure of the discontinuity. The time derivative of the radiation-era scale factor is approximately  $\frac{1}{120}$  of the derivative of the inflationary scale factor. Graph (a) of Figure 2 shows this change in the growth behavior qualitatively. We also note that these values,  $H = 10^{16} \text{ GeV}$  and  $N = 60$ , yield an estimate for the duration of inflation without the need to specify  $t_i$  or  $t_f$ :

$$\Delta t = \frac{N}{H} \approx 4 \times 10^{-39} \text{ s}. \quad (21)$$

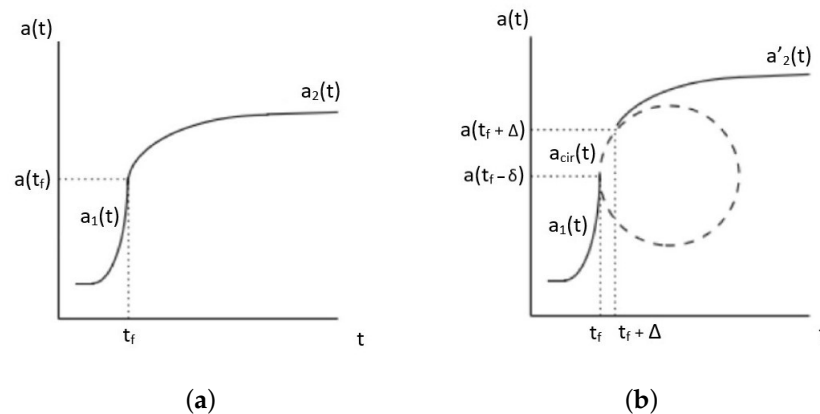


**Figure 2.** (a) The graph depicts the discontinuity between inflationary and radiation-era scale factors at the end of inflation. (b) The circular arc defined by the transitional scale factor  $a_{\text{cir}}(t)$  intersects tangentially with the inflationary scale factor  $a_1(t)$  and the now-displaced radiation-era scale factor noted with a prime,  $a'_2(t)$ . The parameter  $\Delta$  is the time period from the end of inflation until the time of continuity between  $a_{\text{cir}}(t)$  and  $a'_2(t)$ . The  $a$  functions are not to scale.

### 3. The Transition

What kind of transitional function could provide continuity between the two period scale factors? At the end of inflation, the slope begins to decline. For simplicity, we require a steadily declining slope with no regions in which the universe undergoes contraction. This pair of requirements motivates us to conclude that a valid mathematical representation of the physical expansion of space would likely consist of a properly chosen intermediate power law. Expressing the mathematical formalism involves defining a set of parameters for the power law whose values also serve to establish continuity at the points of intersection with the prior inflationary and subsequent single-component-era scale factors. Initially, as demonstrated with Figure 2b, we use a circular arc  $a_{\text{cir}}(t)$ —only to provide a qualitative illustration of the geometry and the set of parameters. In Section 4, we discard the model based on the circular arc, because it is not a realistic physical solution, and focus strictly on evaluating the possible power-law transitions to identify viable candidates.

In Figure 2b, the arc lies tangent to  $a_1(t)$  at the end of inflation and tangent to the now-displaced radiation-era scale factor noted with a prime,  $a'_2(t)$ . The transitional duration  $\Delta$  remains to be determined.

In the more detailed view of Figure 3, we see five unknown variables:

- $R$ —the radius of the circular arc;
- $\Delta$ —the time between  $t_f$  and the tangent point at which the circular arc  $a_{\text{cir}}(t)$  meets the displaced radiation era  $a'_2(t)$ ;
- $a(t_f - \delta)$ —the  $a$ -axis value at  $t_f - \delta$ , aligned with the center of the arc;
- $\delta$ —the measure of the  $t$ -axis displacement corresponding to the difference between  $a(t_f)$  and  $a(t_f - \delta)$ ;
- $a(t_f + \Delta)$ —the scale factor at  $t_f + \Delta$ , the  $t$ -axis point of tangency for  $a_{\text{cir}}(t)$  and  $a'_2(t)$ .

The transitional function is just the equation of the circle

$$a_{\text{cir}}(t) = a(t_f - \delta) + \sqrt{R^2 - [t - (R + t_f - \delta)]^2}. \quad (22)$$

If  $a(t_f)$  and  $a(t_f - \delta)$  were to coincide, we would be introducing another discontinuity into the model, i.e., the change from the inflationary slope to the infinite slope of the circular arc. With the displacement  $\delta$ , the edge of the circular arc lies earlier on the timeline than  $t_f$ , and  $\delta$  sets that duration. We note that  $a(t_f - \delta)$  is, therefore, never the physical value of the scale factor and so has no direct effect on the expansion of space.

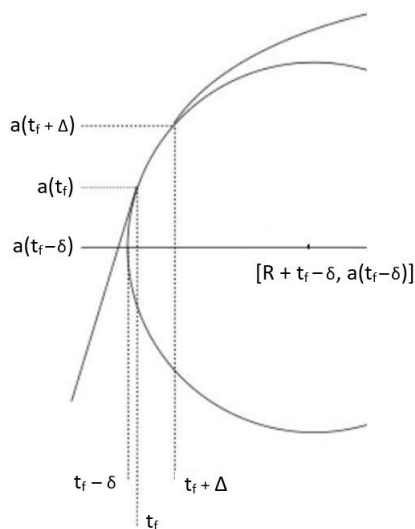


**Figure 3.** Five unknown parameters characterize the two points of tangency of  $a_{\text{cir}}(t)$  with the period scale factors (not to scale).

We establish smoothness by equating the scale factors and their derivatives at the tangency points. Thus, we have five unknown parameters in the four matching conditions. In Section 5.3, we invoke a fifth equation to specify the model completely.

#### 4. Power-Law Transitions

Imposing a circular arc is an unreasonably strict condition to use to define an interpolating function. We shall continue now by exploring more general power-law solutions for  $a(t)$  in the transition between the period scale factors (in fact, just as having the most realistic quasi-equilibrium equation of state would involve including power-law terms with different indices, corresponding to different types of matter content, a more elaborate interpolator could also include a sum of terms with different power-law indices—although we shall not consider functions with that level of generality). Even just a single properly chosen power-law section could provide continuity and also potentially lengthen one or the other of the periods it connects, depending on its orientation. A power law with  $n < 1$  has essentially no impact on the length of the radiation era. For a power law with  $n > 1$ , a very small increase in the inflationary period could have a substantial impact on the scale factor, as discussed further in Section 4.2.

##### 4.1. Interpolating Power Laws with $n < 1$

The power law takes the form

$$a_p(t) = a_p(t_f - \delta) + D [t - (t_f - \delta)]^n. \tag{23}$$

We use the notation  $a_p(t)$  for power laws with  $n < 1$ . The subscript  $p$  denotes the representative parabola for  $n = \frac{1}{2}$ , which opens to the right and has a horizontal axis. The unknown coefficient  $D$  is the analog of the unknown radius of the circular arc. Additional unknown parameters  $a_p(t_f - \delta)$ ,  $\delta$ ,  $\Delta$ , and  $a(t_f + \Delta)$  correspond to the parameters displayed in Figure 3 for the circular arc. We analyze the continuity of the forms of the scale factor at the two points of tangency.

#### 4.1.1. Smoothness at $t_f$

For the first matching condition—continuity of  $a(t)$ —at  $t_f$ ,  $a_p(t)|_{t_f} = a(t_f)$  implies

$$D = \frac{a(t_f) - a_p(t_f - \delta)}{\delta^n} \quad (24)$$

$$a_p(t) = a_p(t_f - \delta) + \frac{a(t_f) - a_p(t_f - \delta)}{\delta^n} [t - (t_f - \delta)]^n. \quad (25)$$

The second matching condition at  $t_f$  equates the time derivatives, generating an expression for the  $a$ -axis vertex coordinate:

$$\dot{a}_p(t)|_{t_f} = \dot{a}_1(t)|_{t_f} = T(t_0) \quad (26)$$

$$\dot{a}_p(t)|_{t_f} = n \left[ \frac{a(t_f) - a(t_f - \delta)}{\delta^n} \right] \delta^{n-1} \quad (27)$$

$$a_p(t_f - \delta) = a(t_f) - \frac{T(t_0)\delta}{n}, \quad (28)$$

where we used the relations in Equations (14) and (18) to express these in terms of the current temperature  $T(t_0)$ , since  $t = t_0$  also provides the calibration scale for  $a$ . With the vertex coordinate from Equation (28), the scale factor is

$$a_p(t) = a(t_f) - \frac{T(t_0)\delta}{n} + \frac{T(t_0)}{n\delta^{n-1}} [t - (t_f - \delta)]^n. \quad (29)$$

#### 4.1.2. Smoothness at $t_f + \Delta$

The interpolating transition we imposed between the end of inflation and the beginning of the radiation era shifts the Equation (13) scale factor according to

$$a'_2(t) = a(t_f + \Delta) \sqrt{\frac{t}{t_f + \Delta}}, \quad (30)$$

where we use the prime to distinguish this shifted expression. The vertex of the radiation-era  $t^{1/2}$  scale factor remains at  $(t = 0, a = 0)$ . The third matching condition, in which the interpolating power law equals  $a'_2(t)$  at the point of tangency, yields the noninformative solution

$$a'_2(t)|_{t_f + \Delta} = a_p(t_f + \Delta). \quad (31)$$

However, the final smoothness condition equates the derivatives of the scale factors  $a'_2(t)$  and  $a_p(t)$  at  $t_f + \Delta$ , so we have

$$\dot{a}_p(t)|_{t_f + \Delta} = \dot{a}'_2(t)|_{t_f + \Delta} \quad (32)$$

$$\dot{a}'_2(t)|_{t_f + \Delta} = \frac{a_p(t_f + \Delta)}{2(t_f + \Delta)} \quad (33)$$

$$\dot{a}_p(t)|_{t_f + \Delta} = \frac{T(t_0)}{\delta^{n-1}} [t - (t_f - \delta)]^{n-1} \Big|_{t_f + \Delta} \quad (34)$$

$$= \frac{T(t_0)}{\delta^{n-1}} (\Delta + \delta)^{n-1}. \quad (35)$$

Thus, we ultimately arrive at the condition

$$\frac{T(t_0)}{\delta^{n-1}} (\Delta + \delta)^{n-1} = \frac{a_p(t_f + \Delta)}{2(t_f + \Delta)} \tag{36}$$

$$\frac{T(t_0)}{\delta^{n-1}} (\Delta + \delta)^{n-1} = \frac{1}{2(t_f + \Delta)} \left[ a(t_f) - \frac{T(t_0)\delta}{n} + \frac{T(t_0)}{n\delta^{n-1}} (\Delta + \delta)^n \right]. \tag{37}$$

The formalism leaves us with the need to fix  $\Delta$  to evaluate the model;  $\Delta$  and  $a(t_f + \Delta)$  are physical but as yet unknown parameters. The others are mathematical constructs with no direct physical meanings. After substituting the early universe parameter values assumed in Section 2.1, we find, for example, the solution for  $n = \frac{1}{2}$  at  $\Delta = 10^{-35}$  s:

$$\delta \approx 2.65 \times 10^{-6} \Delta \tag{38}$$

(evaluated using Maple).

Table 1 lists additional values of  $\delta$  for a sample set of transition durations  $\Delta$ . The purpose of having three significant figures listed in the table is to illustrate the relationship between the displacement and any changes to the transition scale.

**Table 1.** The vertex displacements  $\delta$  for power laws  $a(t) \propto t^{1/2}$  and  $t^2$  for a sample set of transition durations  $\Delta$  between the end of inflation and the beginning of the radiation era. Increasing the duration  $\Delta$  for the power law  $n = \frac{1}{2}$  tends to set the displacement of the vertex. However, because of the difficulty of establishing continuity with the inflationary slope at  $t_f$ , the displacement  $\delta$  for the  $n = 2$  interpolator is many orders of magnitude greater. With its vertex located later on the timeline than  $t_f$ , the table shows that increasing the transition has the effect of shifting the vertex of  $a_v(t)$  farther away from the end of inflation.

Transition	$n$	$\Delta$ (s)	$\delta$ (s)
$a_p(t)$	$\frac{1}{2}$	$10^{-35}$	$2.65 \times 10^{-41}$
		$10^{-33}$	$3.22 \times 10^{-41}$
		$10^{-30}$	$3.29 \times 10^{-41}$
		$10^{-22}$	$3.29 \times 10^{-41}$
$a_v(t)$	2	$10^{-35}$	$1.50 \times 10^{-35}$
		$10^{-22}$	$1.50 \times 10^{-22}$

We accomplished the objective of parameterizing the transition from the inflationary scale factor with a family of power-law scale factors that ensure sufficient smoothness to have continuity of  $a$  and its first time derivative—although we did not impose the condition of continuity on any higher-order derivatives. The slope of the inflation-era scale factor grows at a rate on the order of the Hubble parameter, and a requirement of continuity on the second derivative would effectively extend inflation into the subsequent period, rather than marking the physical end of inflation as the point at which the second derivative becomes negative.

#### 4.2. Power Laws with $n > 1$

To continue the study of alternative transitions, we now examine power laws with  $n > 1$ , containing unknown parameters analogous to those analyzed in the previous section. The scale factor formula is

$$a_v(t) = a_v(t_f + \delta) + E [t - (t_f + \delta)]^n. \tag{39}$$

The subscript  $v$  denotes the representative inverted parabola for  $n = 2$  with the vertical axis parallel to the  $a$ -axis. The displacement of the vertex from  $a(t_f)$  now places  $\delta$  at a time later than the tangent point at  $t_f + \Delta$ , as shown in Figure 4.

Repeating the analysis of the matching conditions at  $t_f$  and  $t_f + \Delta$  yields the scale factor

$$a_v(t) = a(t_f) + \frac{T(t_0)\delta}{n} + \frac{T(t_0)}{n(-\delta)^{n-1}}[t - (t_f + \delta)]^n \tag{40}$$

and a fourth matching condition

$$\frac{T(t_0)}{(-\delta)^{n-1}} (\Delta - \delta)^{n-1} = \frac{1}{2(t_f + \Delta)} \left[ a(t_f) + \frac{T(t_0)\delta}{n} + \frac{T(t_0)}{n(-\delta)^{n-1}} (\Delta - \delta)^n \right]. \tag{41}$$

As Table 1 details for a sample set of transition durations, the vertex displacement  $\delta$  for a power law with  $n = 2$  and  $\Delta = 10^{-35}$  s is almost six orders of magnitude farther from the point of tangency than that of the power law with  $n = \frac{1}{2}$ . The power law  $a_p(t) \propto t^{1/2}$  can establish continuity with the slope of the inflationary scale factor with such a minute displacement, because the power law has an infinite slope at the vertex. However, the power law  $a_v(t) \propto t^2$  has no such infinite slope, and the difficulty of establishing continuity with the large slope at the end of inflation,  $\sim 10^{11} \text{ s}^{-1}$ , manifests itself in the displacement being many orders of magnitude greater than that of  $a_p(t) \propto t^{1/2}$ .

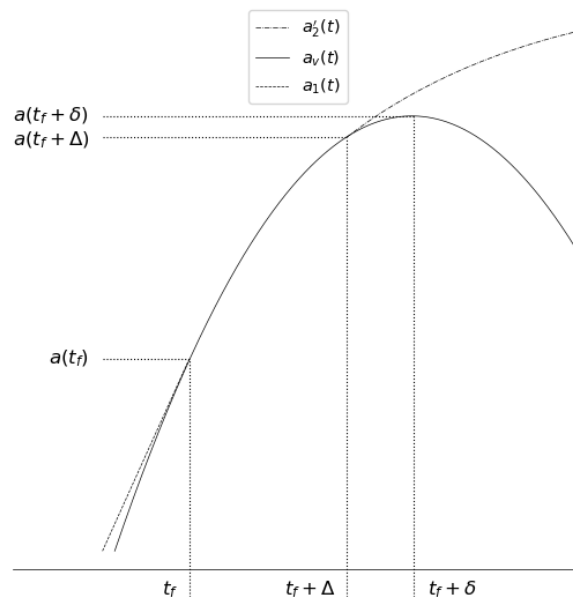


**Figure 4.** The displacement  $\delta$  necessarily places the vertex of the representative inverted parabola with power-law index  $n = 2$  later than the end of inflation at  $t_f$  and the tangency point at  $t_f + \Delta$  (not to scale). Increasing the duration over which the the interpolating scale factor applies also shifts the vertex similarly.

Figure 5 displays the transitional scale factors of Equations (29) and (40), rescaled by a translation of the  $t$ -axis  $t \rightarrow t' = t_f + t$ . The timeline starts at the arbitrarily small initial value  $t = 10^{-43}$  s. The graphs represent power laws for  $n < 1$  and  $n > 1$  with a representative sample of powers. However, the graphs of the scale factors themselves offer somewhat limited insight into the evaluation of the quality of the interpolating functions. For that, we now look instead to graphs of the Hubble parameter:

$$H(t_f + t) = \frac{\dot{a}(t_f + t)}{a(t_f + t)}. \tag{42}$$

In the transitional Hubble parameters below,  $H_{in}$  is the constant inflationary Hubble parameter, taken to be  $10^{16}$  GeV. For the two classes of power laws, we find

$$H_p(t_f + t) = \frac{(1 + \frac{t}{\delta})^{n-1}}{\frac{1}{H_{in}} - \frac{\delta}{n} + \frac{\delta}{n}(1 + \frac{t}{\delta})^n} \tag{43}$$

$$H_v(t_f + t) = \frac{(1 - \frac{t}{\delta})^{n-1}}{\frac{1}{H_{in}} + \frac{\delta}{n} - \frac{\delta}{n}(1 - \frac{t}{\delta})^n} \tag{44}$$

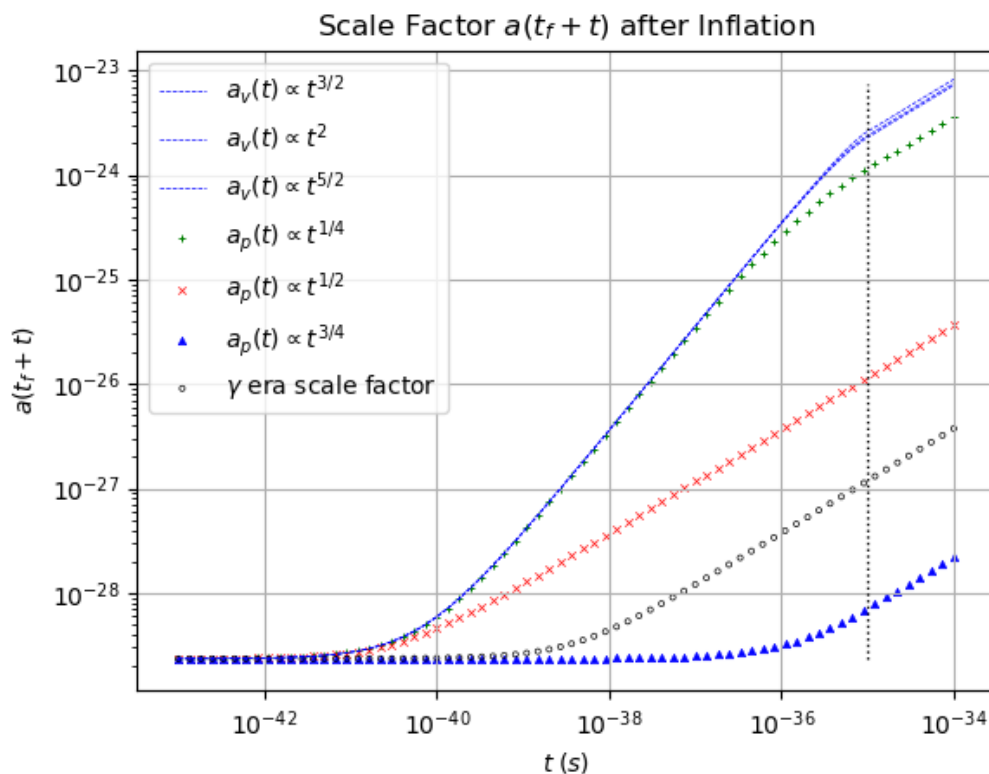


**Figure 5.** The three  $a_v(t)$  scale factors with power laws  $t^{3/2}$ ,  $t^2$ , and  $t^{5/2}$  essentially overlay each other, and the  $a_p(t)$  scale factor proportional to  $t^{1/4}$  approaches those of the power laws with  $n > 1$ . The graph also shows the unsmoothed scale factor defined by Equation (13), which exceeds that of  $a_p(t)$  at  $t^{3/4}$ . The  $t$ -axis timeline begins at  $t = 10^{-43}$  s after inflation terminates, while the vertical dotted line at  $t = 10^{-35}$  s marks the nominal start of the radiation era.

In Figure 6, showing graphs of Equations (43) and (44), we note that the requirement of smoothness at the beginning of the radiation era causes abrupt shifts downward and upward as  $t \rightarrow \Delta$  for interpolating scale factors not proportional to  $t^{1/2}$ . We note that the power laws with  $n > 1$  that overlay each other in both Figures 5 and 6 must exhibit the shift downward to establish continuity with the radiation-era Hubble parameter. Unable to justify a physical basis for this behavior, we shall move forward in our analysis by eliminating these power laws as valid interpolating functions and focus on more specifically determining workable interpolating functions with  $n < 1$ . We also note that as  $n \rightarrow \frac{1}{2}$  from above or below, the scale factor  $a_p(t)$  transforms more seamlessly into the radiation era. Thus, at this stage, we expect that the most suitable interpolating functions will correspond to the index value  $n = \frac{1}{2}$ , or something close to that. The power laws for the interpolating region and the subsequent radiation-dominated era are both horizontally opening parabolas (or nearly so), which differ principally in their vertex placements and radii of curvature.

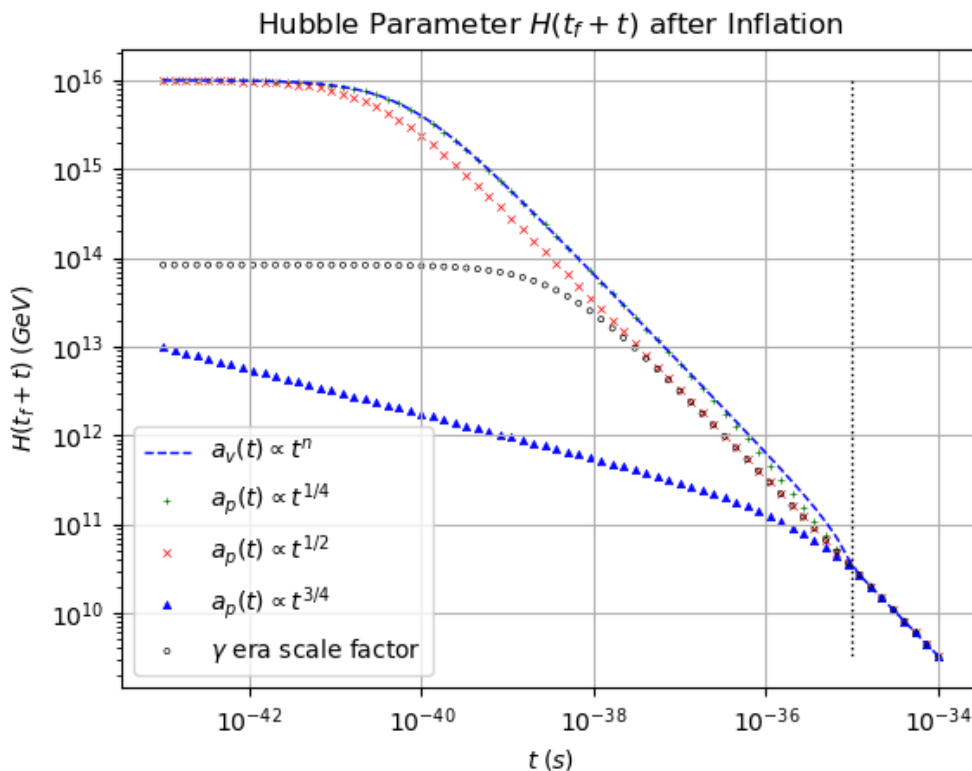


**Figure 6.** The Hubble parameters corresponding to the scale factors shown in Figure 5. Once again, the graphs based on the scale factors  $a_v(t)$  for  $t^{3/2}$ ,  $t^2$ , and  $t^{5/2}$  essentially overlay each other. The discontinuity of the radiation-era Hubble parameter with  $H_{in}$  exceeds two orders of magnitude. The graph based on scale factor  $a_p(t)$  for  $t^{3/4}$  fails to display asymptotic behavior with  $H_{in}$  at small times, because the timeline has the same  $t$ -axis translation and does not start at  $t_f$ . Again, the vertical dotted line marks the start of the radiation era at  $t = 10^{-35}$  s.

### 5. Additional Constraints

#### 5.1. The Equation of State

We continue with the evaluation of the usefulness of the possible interpolations by considering a parameter  $\epsilon_H$ , which is an alternative to the equation-of-state parameter  $\omega$  that satisfies  $p = \omega\rho$ , according to

$$\epsilon_H = \frac{d \log(H^{-1})}{d \log a} = \frac{3}{2}(1 + \omega). \tag{45}$$

Following a graphical technique described by Kaloian Lozanov [26], we shall interpret the formula as the slope in a plot of the evolution of the scale factor from inflation through reheating, matter domination, and finally, the dark-energy-dominated era. Appendix B provides more information about this expression. Figure 7 shows our version of the Lozanov graphical approach for the power law  $a_p(t) \propto t^n$ , with  $n$  ranging from 0.05 to 0.95. Table 2 lists statistics for some of the graphed power laws, and smaller and larger values of  $n$ .

Aside from the footnoted observations in Table 2, we note a further curious feature of Figure 7. The graphs at the upper and lower extremes of  $n$  display almost cusp-like changes of slope at the tangent point between the transition and the radiation-dominated era at  $t = t_f + \Delta$ . Between inflation and the start of the radiation-dominated era,  $\epsilon_H$  changes from a value much greater than 2 to less than 2 for  $n > \frac{1}{2}$ . Conversely, for  $n < \frac{1}{2}$ , the parameter starts at less than 2 and then becomes greater than 2. With our expectation that  $\epsilon_H = 2$ , only the power law  $n = \frac{1}{2}$  (the same power-law index as in the radiation era itself) appears

able to transition seamlessly to the radiation era, which suggests that all powers except  $n = \frac{1}{2}$  result in a cusp in the evolution of  $\epsilon_H$ . This motivates a closer inspection.

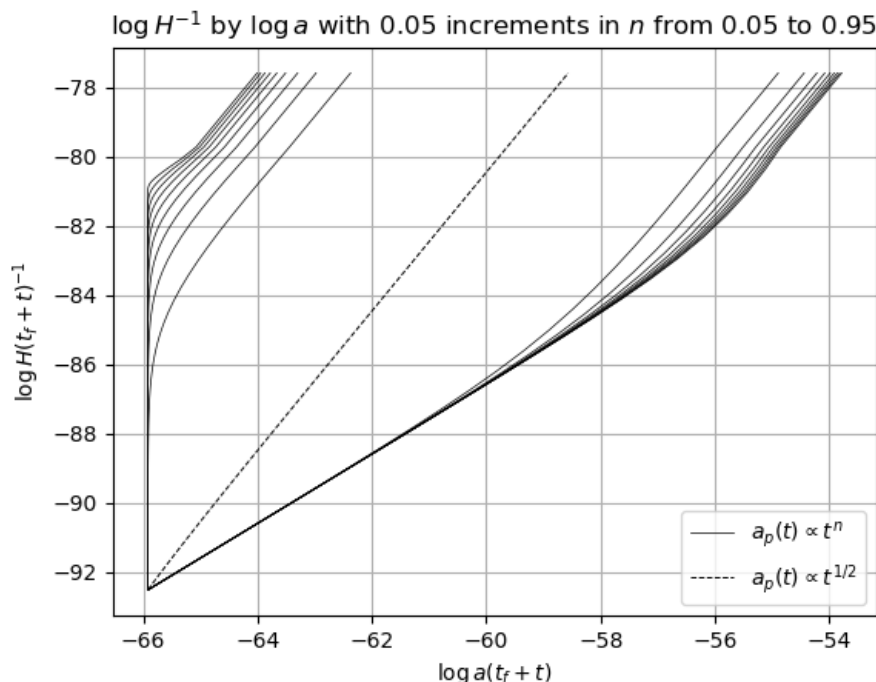


Figure 7. The slopes of the graphs equal the parameter  $\epsilon_H = \frac{d \log(H^{-1})}{d \log a}$ .

**Table 2.** The displacement  $\delta$ , parameter  $\epsilon_H$ , and equation-of-state parameter  $\omega = \frac{2}{3}\epsilon_H - 1$  for power laws  $a_p(t) \propto t^n$ , with values of  $n$  ranging between 0 and 1. (a) Computation sets this value more precisely at  $\approx 2.00039$ . After interpolation using the linear relation associated with Equation (46), the expected  $\epsilon_H = 2$  for a radiation-dominated scale factor occurs at  $n \approx 0.5002$ . (b) Values of  $\epsilon_H \rightarrow 2.6^-$  and  $\omega \approx 0.73$  signify unphysical, exotic tachyon-like particles with velocities greater than the speed of light, which Section 5.2 discusses in detail. (c) For  $\epsilon_H \approx 1.50$  and  $\omega \approx 0.00$ , we have a transition from inflation to an equation of state that would be consistent with a matter-dominated universe. We take up consideration of the single-component matter-dominated universe in Section 5.3. (d) As  $\epsilon_H \rightarrow 1.0^+$  and  $\omega \rightarrow -\frac{1}{3}$ , the scale factor remains inflationary, effectively eliminating the transition.

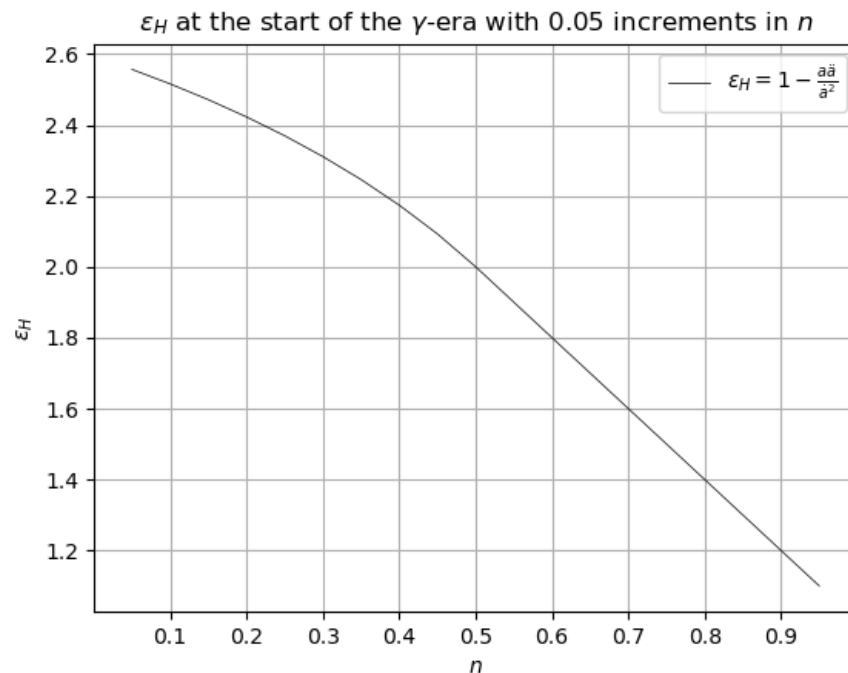
$n$	$\delta$ (s)	$\epsilon_H$	$\omega$
0.002	$2.53 \times 10^{-36}$	2.59	0.73 <sup>(b)</sup>
0.25	$9.55 \times 10^{-37}$	2.37	0.58
0.50	$2.65 \times 10^{-41}$	2.00 <sup>(a)</sup>	0.33
0.75	$9.46 \times 10^{-56}$	1.50	0.00 <sup>(c)</sup>
0.98	$2.31 \times 10^{-294}$	1.04	-0.31 <sup>(d)</sup>

Figure 8 plots  $\epsilon_H$  versus the power-law index  $n$  at time  $(t_f + \Delta)$ :

$$\epsilon_H = 1 + (1 - n) \frac{a(t_f) - \frac{T(t_0)\delta}{n} + \frac{T(t_0)\delta}{n} \left(1 + \frac{\Delta}{\delta}\right)^n}{T(t_0)\delta \left(1 + \frac{\Delta}{\delta}\right)^n}. \tag{46}$$

For  $n > \frac{1}{2}$ , the negative term in the numerator of Equation (46) is small relative to the other terms appearing in the fraction, which are on the order of  $a(t_f)$  and essentially cancel with the factor of the same characteristic size in the denominator. The linear relation  $\epsilon_H - 1 \propto (1 - n)$  remains, as the graph and Table 2 show. In contrast, for  $n < \frac{1}{2}$ , the scale

factor  $a(t_f)$  is small relative to the other terms in the fraction. As  $n \rightarrow 0$ , the fraction and  $(1 - n)$  are both increasing, and  $\epsilon_H$  increases to approximately 2.6.



**Figure 8.** The parameter  $\epsilon_H = -\frac{\dot{H}}{H^2}$  with power law  $a_p(t) \propto t^n$  for  $n < 1$  at the start of the radiation era, with the transition period  $\Delta = 10^{-35}$  s.

Figure 8 aligns with the possibility raised by Figure 5 that only  $n = \frac{1}{2}$  results in a transition to the radiation era without an awkward, cusp-like feature—whose very presence would seem to be contrary to the dictum we adopted of modeling the transitions in a smooth fashion. However, precise calculations consistently indicate that a slightly different  $n \approx 0.5002$  actually produces the seamless transition. In the same way as the abrupt shift that we cannot explain in the graph of the Hubble parameters tends to disqualify all power laws except  $n = \frac{1}{2}$ , the cusp-like features again appear likely to signify unphysical, unexplained behavior. However, before we attempt to resolve these conflicts, we shall review additional constraints on the equation of state, starting with constraints related to the speed of sound.

### 5.2. Speed of Sound Constraints

Another tool for evaluating the interpolators is the application of constraints on the speed of sound to the equation of state. A speed of sound less than zero or greater than the speed of light would violate stability or causality, respectively [29,30]. Stability requires that the speed must be real; imaginary phase speeds would correspond to imaginary frequencies, or modes that grow exponentially with time. At the other end, special relativity imposes the standard limitation that information carried by arbitrary quanta cannot propagate faster than the speed of light  $c = 1$  in a vacuum. Thus, we expect the sound speed of the transition waves to obey inequalities

$$0 \leq v_s^2 \leq 1. \quad (47)$$

We assume, as is standard, that the inflaton wave oscillations are fast and, thus, adiabatic, so that a passing wave brings about temperature changes without conductive heat transfer. The thermodynamic behavior is reversible, and so the entropy per unit mass is constant [31] as an inflaton wave passes through. Pressure  $p = p(s, \rho)$  becomes a function of the density  $\rho$  only:  $p = p(\rho)$ . We also make the assumption that the inflaton condensate at the end of inflation is a perfect fluid, allowing us to apply a linear, single-component

equation of state,  $p = \omega\rho$ , expressing the dependence of pressure on density in terms of a  $\rho$ -independent equation-of-state parameter  $\omega$ . This environment yields a sound speed

$$v_s^2 = \frac{1}{d\rho/dp} = \frac{dp}{d\rho} = \omega, \tag{48}$$

and using  $\omega = \frac{2}{3}\epsilon_H - 1$ , the condition  $0 \leq \omega \leq 1$  implies  $\frac{3}{2} \leq \epsilon_H \leq 3$ . At the precise end of inflation,  $\Delta = 0$  in Equation (46), leaving

$$\epsilon_H = 1 + (1 - n) \frac{a(t_f)}{T(t_0)\delta} = 1 + \frac{(1 - n)}{H\delta}. \tag{49}$$

Figure 9 displays the effect of enforcing the sound speed restrictions from Equation (47) on  $\epsilon_H$ ; these conditions severely restrict the permissible range of power-law indices. The line plot is a Python cubic spline interpolation of Maple-generated solutions for the parameter  $\epsilon_H$  from Equation (46) in 0.001 increments around  $n = \frac{1}{2}$ . The section of the spline interpolation within the gray horizontal band contains valid values of  $\epsilon_H$ , corresponding to interpolating theories with stable, causal sound speeds. Reading off the graph, we see the permissible physical power-law band for the continuous function transitioning from the end of inflation to the radiation era lies approximately between  $0.4990 < n < 0.5005$ . This narrow band is consistent with the large separation in Figure 7 between the power law  $n = \frac{1}{2}$  and the closely adjacent powers  $n = 0.45$  and  $n = 0.55$ .

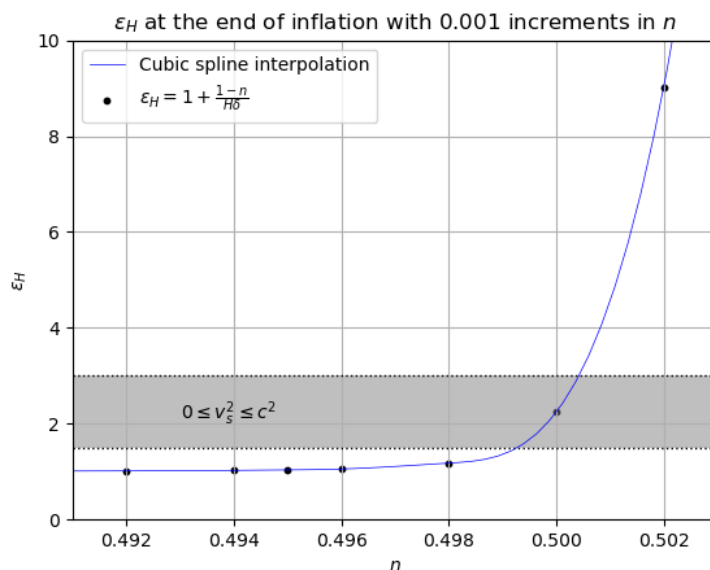


**Figure 9.** Values of the parameter  $\epsilon_H = 1 + \frac{(1-n)}{H\delta}$  at the end of inflation,  $t_f \approx 4 \times 10^{-39}$  s, for  $a_p(t) \propto t^n$  with  $n \approx \frac{1}{2}$ . The gray band depicts the permissible values of  $\epsilon_H$ ,  $\frac{3}{2} \leq \epsilon_H \leq 3$ , subject to the assumption that the inflaton condensate at the end of inflation is a single-component perfect fluid with the equation of state  $p = \omega\rho$ .

### 5.3. Continuity of the Equation of State

Although we found restrictions on the allowed range of power-law values, a tension between the expected and derived equations of state for  $n = \frac{1}{2}$  actually remains. We do not find that  $\epsilon_H = 2$  corresponds exactly to  $n = \frac{1}{2}$ . We instead recall the expected  $\epsilon_H = 2$  was associated with  $n \approx 0.5002$  reported in Table 2, and we now seek to understand the reason for the slight discrepancies between these values and the derived  $\epsilon_H \approx 2.00039$  that corresponds to the exact  $n = \frac{1}{2}$ .

A comparison of the scale factor in Equations (28) and (29) of Section 4.1 with the first two terms in the numerator of the fraction in the expression below:

$$\epsilon_{H \text{ derived}} = 1 + (1 - n) \frac{a(t_f) - \frac{T(t_0)\delta}{n} + \frac{T(t_0)\delta}{n} \left(1 + \frac{\Delta}{\delta}\right)^n}{T(t_0)\delta \left(1 + \frac{\Delta}{\delta}\right)^n}, \tag{50}$$

indicates that those two terms arise from the  $a$ -axis scale factor displacement  $a_p(t_f - \delta)$  of the interpolating function’s vertex. The third term in the numerator represents the functional dependence of the scale factor on time.

Table 3 separates the difference between the expected and derived  $\epsilon_H$  into the relative contributions from the components of the numerator:  $\epsilon_{H \text{ displacement}}$  and  $\epsilon_{H \text{ time}}$ . For comparison, we repeat the analysis for a single-component, matter-dominated transition function establishing continuity between the end of inflation and a matter-dominated era (that is, with  $n = \frac{2}{3}$  power laws). We can see the results are qualitatively the same. The displacement of the vertex of the scale factor along the  $a$ -axis is responsible for the discrepancies.

**Table 3.** These parameters correspond to power laws  $a_p(t)$  with indices  $n = \frac{1}{2}$  and  $n = \frac{2}{3}$  transitioning to radiation-dominated and matter-dominated eras with scale factors similarly proportional to  $t^{1/2}$  and  $t^{2/3}$ . The column  $\epsilon_{H \text{ derived}}$  reconstructs the parameter as the sum of 1 and the contribution from the displacement and the time components. We conclude that the displacement causes the difference from  $\epsilon_{H \text{ expected}}$ .

$n$	$\delta$ (s)	$\epsilon_{H \text{ expected}}$	$\epsilon_{H \text{ derived}}$	$\epsilon_{H \text{ displacement}}$	$\epsilon_{H \text{ time}}$
$\frac{1}{2}$	$2.65 \times 10^{-41}$	2	2.00039	0.00039	1.00000
$\frac{2}{3}$	$7.71 \times 10^{-42}$	1.5	1.50020	0.00020	0.50000

If not for the contribution of the vertex displacement, we would have seamless transitions of the equation of state between the interpolating power laws and the radiation or matter eras. A first-order phase transition at  $(t_f + \Delta)$  might be responsible for the cusp, but we reason against that possibility. The dynamics of the expansion of space at the tangent point undergoes no change. Prior to and after  $(t_f + \Delta)$ , the power-law index  $n$  governing expansion remains approximately the same for each single-component era. Also, the transition precedes the period of preheating described in Section 7 and subsequent thermalization, so that we expect the temperature to evolve smoothly at  $t_f + \Delta$ .

Instead, invoking continuity of the equation of state at  $(t_f + \Delta)$  and noting  $\epsilon_{H \text{ expected}} = \frac{1}{n}$  for a single-component universe, as Appendix C shows, we solve Equation (50) for the displacement  $\delta$  and find

$$\epsilon_{H \text{ expected}} = \frac{1}{n} = 1 + (1 - n) \frac{a(t_f) - \frac{T(t_0)\delta}{n} + \frac{T(t_0)\delta}{n} \left(1 + \frac{\Delta}{\delta}\right)^n}{T(t_0)\delta \left(1 + \frac{\Delta}{\delta}\right)^n} \tag{51}$$

$$\frac{1}{n} = \frac{a(t_f) - \frac{T(t_0)\delta}{n} + \frac{T(t_0)\delta}{n} \left(1 + \frac{\Delta}{\delta}\right)^n}{T(t_0)\delta \left(1 + \frac{\Delta}{\delta}\right)^n}. \tag{52}$$

Substituting  $a(t_f) = T(t_0)/H$  from Equation (18) with  $H = H_{\text{in}}$  yields

$$\delta = \frac{n}{H}. \tag{53}$$

An analysis of Equation (50) demonstrated that the displacement

$$\epsilon_{H \text{ displacement}} = a(t_f) - \frac{T(t_0)\delta}{n} \tag{54}$$

caused the cusp-like feature. With the Equation (53) result, and recalling  $a(t_f) = \frac{T(t_0)}{H}$ , we instead have  $\epsilon_H \text{displacement} = 0$ , and the bump on the curve is gone.

However, making the assumption of continuity of the equation of state at  $t_f + \Delta$  destroys the smoothness of the scale factor that we imposed at both  $t_f + \Delta$  and  $t_f$ . Thus, we must re-examine the matching condition at  $t_f + \Delta$ ; returning to the fourth matching condition and trying to solve for  $\Delta$ , we see that

$$\frac{T(t_0)}{\delta^{n-1}} (\Delta + \delta)^{n-1} = \frac{1}{2(t_f + \Delta)} \left[ a(t_f) - \frac{T(t_0)\delta}{n} + \frac{T(t_0)}{n\delta^{n-1}} (\Delta + \delta)^n \right] \quad (55)$$

$$T(t_0) \left( 1 + \frac{\Delta}{\delta} \right)^{n-1} = \frac{1}{2(t_f + \Delta)} \left[ \frac{T(t_0)}{H} - \frac{T(t_0)\delta}{n} + \frac{T(t_0)\delta}{n} \left( 1 + \frac{\Delta}{\delta} \right)^n \right] \quad (56)$$

$$0 = \frac{1}{H} - \frac{\delta}{n} + \frac{\delta}{n} \left( 1 + \frac{\Delta}{\delta} \right)^n - 2(t_f + \Delta) \left( 1 + \frac{\Delta}{\delta} \right)^{n-1}. \quad (57)$$

With  $\delta = \frac{n}{H}$ , this simplifies to

$$2(t_f + \Delta) = \frac{1}{H} \left( 1 + \frac{H\Delta}{n} \right) \quad (58)$$

$$\Delta = \frac{\frac{1}{H} - 2t_f}{2 - \frac{1}{n}}. \quad (59)$$

Thus, the transition period  $\Delta$  is undefined for  $n = \frac{1}{2}$ , which invalidates the claim of first-derivative smoothness imposed by the Equation (38) parameters,  $\delta \approx 2.65 \times 10^{-6}\Delta$ . For  $n \approx 0.5002$ , associated with  $\epsilon_H = 2$ , the new formula's value of  $\Delta$  is in fact less than zero. Since  $\Delta$  is supposed to represent the length of time over which the interpolating function applies, this value is manifestly unphysical.

Furthermore, substituting  $\delta = n/H$  in the interpolating scale factor:

$$a_p(t) = a(t_f) - \frac{T(t_0)\delta}{n} + \frac{T(t_0)\delta}{n} \left( 1 + \frac{t - t_f}{\delta} \right)^n \quad (60)$$

$$= \frac{T(t_0)\delta}{n} \left( 1 + \frac{t - t_f}{\delta} \right)^n, \quad (61)$$

eliminates the  $a$ -axis displacement of  $a_p(t)$ . We introduced the displacement of the power-law vertex in Section 4.1.1 in order to enforce the smoothness condition at  $t_f$ , but this would be undone by the assumption of exact continuity of the equation of state.

The Lozanov graphical approach to analyzing the equation of state suggests a range of power-law indices,  $0.5000 \lesssim n \lesssim 0.5002$ , are reasonable, and this is supported by the values they are permitted by the speed-of-sound constraints  $0.4990 \lesssim n \lesssim 0.5005$ . Having tried unsuccessfully to establish continuity with the equation of state at  $t_f + \Delta$ , we now seek an explanation of the discontinuity. If the transition represents a continuation and ultimately a termination of inflation, a local discontinuity might result from a weak phase transition of unknown character. A second explanation may be that a power-law index not equal to 0.5 in the transition signals that the composition of the universe is not strictly radiation-dominated as the transition ends, and so a single-component model is not sufficient to describe the dynamics.

## 6. Summary of Numerical Results

We found that a transition function with power-law index  $n$  can provide seamless first-derivative smoothness over the period between the end of inflation and the development of a single-component  $n$ -era universe, while obeying fundamental stability and causality constraints. During the transition, the scale factor increases by approximately an order of magnitude more, compared with what it would have been in a model with a sharp cusp dividing the inflationary from postinflationary functional forms; and that

additional accumulated expansion factor remains as time progresses. Figure 10 shows the key comparisons.

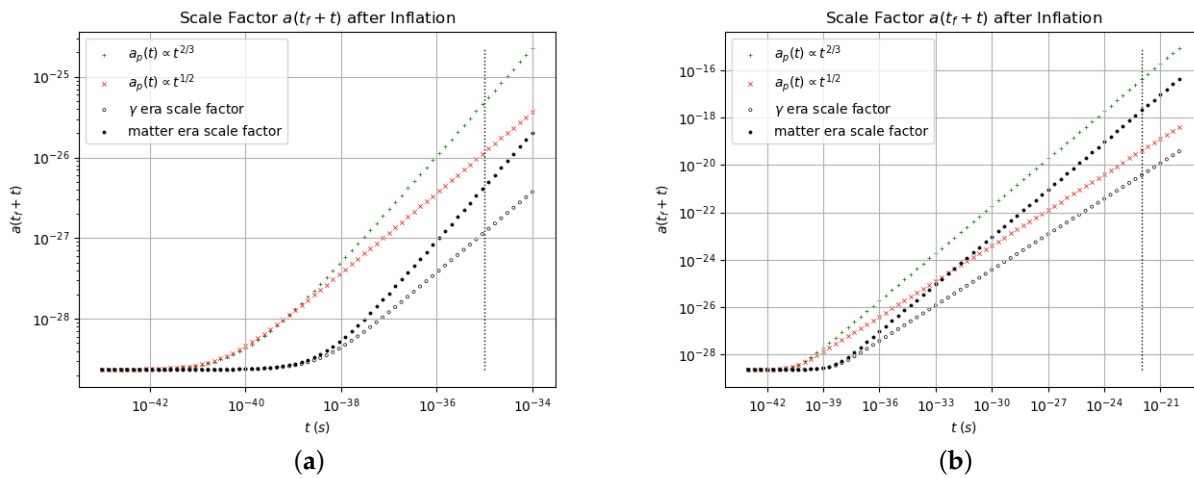


**Figure 10.** The growth in scale factors for single-component universes with smoothness enforced at  $t_f + \Delta$  with  $\Delta = 10^{-35}$  s and  $10^{-22}$  s in (a,b), respectively. We note that the approximate order-of-magnitude increases in the power-law scale factors occur at around  $10^{-37}$  s in all cases.

Figure 11 depicts the increases toward asymptotic limits more clearly. Both Figures 10 and 11 also reveal that these increases occur primarily in the vicinity of  $t = 10^{-37}$  s and do not particularly depend on the duration of the transition  $\Delta$ . Table 4 contains further data, including how much larger, relatively speaking, the universes with the smooth interpolations are than the models without smoothing. The underlying numbers show that after  $10^{-34}$  s, the asymptotic values 9.8 and 11.2 have completely stabilized (to over 12-decimal-place precision). Even by  $10^{-37}$  s, the increased expansion factors have already grown to be within 2% of their asymptotic values.

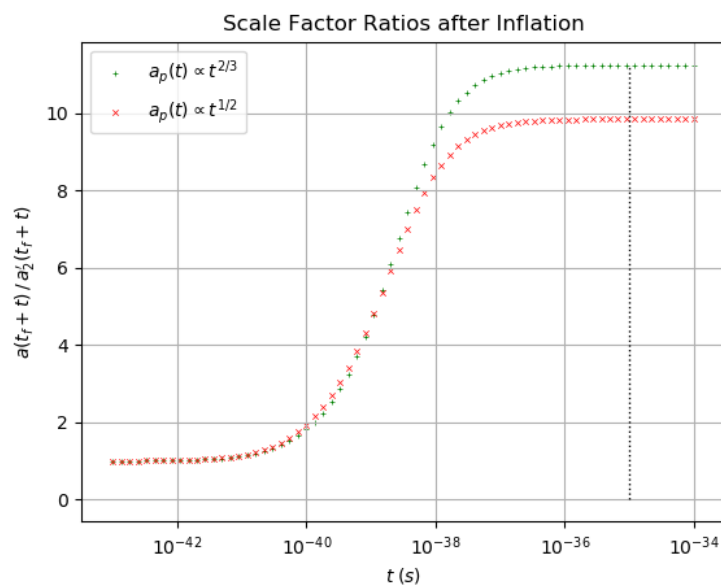


**Figure 11.** The scale factor ratios  $\frac{a_p(t)}{a_2'(t)}$ . At approximately  $t = 10^{-37}$  s, the ratios reach greater than 98% of the asymptotic values of 9.8 and 11.2 for  $a_p(t) \propto t^{1/2}$  and  $a_p(t) \propto t^{2/3}$ , respectively.

**Table 4.** The ratios of  $a_p(t)$  to  $a'_2(t)$  at different times during the interpolation period. The percentages represent the degree to which the ratios have approached the asymptotic values reached at  $10^{-34}$  s.

Time (s)	$a_p(t) \propto t^{1/2}$		$a_p(t) \propto t^{2/3}$	
	Ratio	%	Ratio	%
$10^{-34}$	9.837	100	11.227	100
$10^{-36}$	9.828	99.9	11.217	99.9
$10^{-37}$	9.69	98.5	11.03	98.3
$10^{-38}$	8.4	85.8	9.4	83.3

We are left with the interesting result about what happens when we insert an interpolating function after the end of inflation to smooth out the dynamics. Compared with the models with discontinuous derivatives—signifying abrupt transitions between the inflationary period and a period with a different equation of state—the total expansion of the scale factor is greater by about an order of magnitude (or between 2 and 3  $e$ -folds). In a way, this is unsurprising, since the interpolating function allows the inflationary expansion to tail off a bit more gradually, and so the net result is always a larger universe at later times. This kind of increase in the scale factor will form the basis for our analysis of the effect of continuity in the numerical analysis going forward.

## 7. The Smooth Scale Factor in the Preheating Model

Having concluded that enforcing a smooth transition results in an order-of-magnitude increase in the ultimate scale factor of the subsequent single-component universe, we shall now examine the effects of this change on reheating, based on the preheating model of KLS [22], in which the inflaton couples to a second scalar field  $\chi$  in the era following inflation, which is taken to be a matter-dominated universe. We shall evaluate preheating effects using a smooth interpolating power law with  $n = \frac{2}{3}$ , as described previously in Section 4.1 as an example of a power law with  $n < 1$ . We compare our results to those of the KLS model, which employs the scale factor  $a(t) \approx a_f(t/t_f)^{2/3}$  with a discontinuous slope. Our numerical analysis shows that the larger scale factor in the smooth model decreases the  $\chi$  occupation numbers  $n_k$  and dilutes the total number density  $n_\chi$ . The dilution arises naturally out of the volume increase due to the greater expansion of space—although the broad parametric resonance during preheating partially offsets the effect. Broad parametric resonance involves all modes of the scalar field  $\chi$  less than a specific maximum being involved in quasi-resonant interactions with the inflaton, and it causes an exponential increase in the number of  $\chi$  particles created.

### 7.1. Occupation Numbers

In this section and Section 7.2, we briefly summarize the foundations of the detailed, extensive case that KLS present in support of their theory. The Lagrange density for the scalar field  $\chi$  coupled to the inflaton:

$$\mathcal{L} = -\frac{1}{2}\chi_{,\mu}\chi^{,\mu} - \frac{1}{2}m_\chi^2\chi^2 - \frac{1}{2}g^2\phi^2\chi^2, \quad (62)$$

in expanding space with vanishing mass parameter  $m_\chi = 0$ , generates the equation of motion

$$\ddot{\chi}_k + \frac{3\dot{a}}{a}\dot{\chi}_k + \left(\frac{k^2}{a^2} + g^2\phi^2\right)\chi_k = 0, \quad (63)$$

where  $k = \sqrt{\mathbf{k}^2}$ , for the Fourier mode  $\chi_k$  in momentum space. The inflaton at the end of inflation is a coherently oscillating field of form  $\phi(t) = \Phi(t)\sin(mt)$ , with amplitude envelope  $\Phi(t) = \frac{M_p}{\sqrt{3\pi}mt}$  [24], so that

$$\ddot{\chi}_k + \frac{3\dot{a}}{a}\dot{\chi}_k + \left[\frac{k^2}{a^2} + g^2\Phi^2(t)\sin^2(mt)\right]\chi_k = 0. \quad (64)$$

In slow-roll inflation, chaotic inflation, and other inflationary models in which the friction term  $3H\dot{\phi}$  in the equation of motion (1) becomes negligible, the inflaton exhibits sinusoidal oscillating behavior around  $\phi = 0$  (here the argument of the sine function has time  $t$  in units of  $m^{-1}$ , which the KLS model uses throughout). The appearance of the Planck mass  $M_P$  in  $\Phi(t)$  derives from the Hubble parameter expressed in terms of the gravitational constant. The units of  $k$  are  $m$ , and the scale factor, normalized in the Robertson–Walker metric with  $a(t_0) = 1$  today, remains dimensionless.

Broad parametric resonance consists of nonadiabatic oscillation of the  $\chi$  field in Fourier-space regions where the equation of motion is unstable. The character of the instability is revealed by converting Equation (64) into the standard Mathieu equation. Rescaling the scalar field:

$$X_k = a^{3/2}\chi_k, \quad (65)$$

eliminates the friction-like term and so yields

$$\ddot{X}_k + \left[ \frac{k^2}{a^2} + g^2\Phi^2(t)\sin^2(mt) \right] X_k = 0. \quad (66)$$

Now, recasting the argument of the oscillating term by setting  $z = mt$  completes the conversion into the Mathieu equation:

$$X_k'' + [A_k + 2q\cos(2z)]X_k = 0. \quad (67)$$

The prime represents the derivative with respect to the argument  $z$ , and the two parameters in the equation are

$$A_k = \frac{k^2}{a^2 m^2} + 2q, \quad q = \frac{g^2\Phi^2(t)}{4m^2}. \quad (68)$$

The resonance behavior of solutions to the Mathieu equation depends on the values of these  $A_k$  and  $q$ , which determine the stable and unstable regions. Appendix D reproduces the standard plot depicting the stability and instability regions in the  $q$ - $A_k$  plane with a graph of the Mathieu equation parameters.

The oscillations of the scalar field exhibit adiabatic instability when

$$\frac{\dot{\omega}}{\omega^2} \gtrsim 1, \quad (69)$$

and energy transfer occurs between the inflaton and the scalar field  $\chi$ . Trial solutions of the Mathieu equation:

$$X_k \propto e^{\mu_k z}, \quad (70)$$

are unstable for real values of the Floquet characteristic exponent  $\mu_k$  [32,33]. Section 7.2 discusses  $\mu_k$  in more detail.

The mode occupation number  $n_k$  is the energy of the mode in question, divided by the single-particle energy  $\omega_k$ :

$$n_k = \frac{\omega_k}{2} \left( \frac{|\dot{X}_k|^2}{\omega_k^2} + |X_k|^2 \right) - n_{k0}. \quad (71)$$

(The adjustment  $-n_{k0}$  to account for the zero-point energy density is effectively negligible).

Figure 12 reproduces the results of the discontinuous scale factor of the KLS model, for the scalar field mode amplitude  $X_k$  and the exponential increase in the corresponding occupation number  $\log n_k$ . The  $t$ -axis timeline of both graphs becomes a count of the number of oscillations of the inflaton after  $t$  is expressed in units of  $\frac{2\pi}{m}$ , with which the revised equation of motion (66) is

$$\ddot{X}_k + (2\pi)^2 \left[ \frac{k^2}{a^2} + g^2\Phi^2(t)\sin^2(2\pi t) \right] X_k = 0. \quad (72)$$

Broad parametric resonance preheating requires certain preconditions on  $\Phi(t)$  and the Mathieu equation parameter  $q$ , and it begins shortly after the end of inflation, after approximately one quarter of an oscillation of the inflaton (KLS use this approximation to advance their analysis). With time defined in terms of the number of oscillation cycles,  $t_f = \frac{\pi}{2m} \approx 10^{-37}$  s, which makes the timeline consistent with that which we found for the continuous scale factor, our order-of-magnitude increase in the size of the cosmos also appears at around  $10^{-37}$  s.

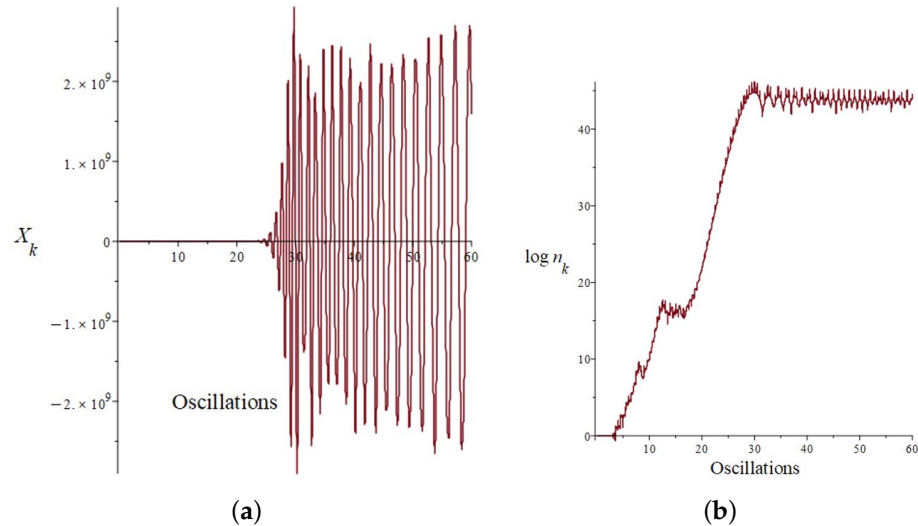


**Figure 12.** (a) The scalar field and (b) occupation number for the first 60 oscillations, in the model with a cusped scale factor, and for the inflaton mass  $m = 10^{-6} M_P$ . The  $t$ -axis is in units of the number of oscillations,  $2\pi/m$ . We selected the specific mode of the KLS model with the wave number  $k = 4m$  to maximize the growth of the occupation number. To reproduce the broad-resonance exponential growth, we used parameters  $g = 6.25 \times 10^{-4}$ ,  $\dot{X}(t_f) = 0.045$ , and  $\ddot{X}(t_f) \approx 0$ ; these were identified empirically, and varying the parameter values away from these will decrease the observable resonance effect. The scalar field derivative  $\dot{X}(t_f)$  approximates what KLS advise—namely, that the positive-frequency solution  $X_k(t) \approx \exp(-i\omega_k t / \sqrt{2\omega_k})$  be applied as an initial condition.

In Figure 12b, the scalar field spans many instability bands in the first  $\sim 10$  oscillations, as  $q$  decreases substantially, and the resonances cause exponential growth in the occupation number. From about 12 to 17 oscillations, the growth flattens as  $q$  lessens while crossing the stability region corresponding to  $q$  values decreasing from about 2 to 1. Broad resonance and growth resume in the next 10 oscillations in the instability band for  $q \lesssim 1$  and  $A_k \approx 1$ , before ultimately terminating after  $\sim 34$  oscillations. Appendix D also shows graph (b) of Figure 12 superimposed on the final three instability regions of Figure A1 (corresponding to decreasing  $q$  as time progresses).

In Figure 13, we repeat the presentation from Figure 12 using the smooth transitional scale factor in place of the kinked scale factor of the KLS model. The scalar field and occupation number show sharp decreases from Figures 12 and 13. We can examine the effect of the continuous scale factor more precisely by analyzing the root mean squares of  $X_k$  and  $n_k$  averaged over the 10 oscillations following the end of preheating, which occurs after approximately 34 oscillations. With time  $t$  in units of  $m^{-1}$  according to the KLS formalism, we can convert the scale factor units of time in seconds to oscillations:

$$a(t) \approx \left[ \frac{t(\text{s})}{t_f} \right]^{2/3} = \left[ \frac{t(\text{s}) \left( \frac{2\pi/m}{\text{s}} \right)}{\frac{\pi}{2m}} \right]^{2/3} = (4t)^{2/3}. \quad (73)$$

We also used the assumption for  $t_f$  that broad parametric preheating begins after inflation ends, at one fourth of an oscillation. Then, we apply a factor of 10 for the approximate order-of-magnitude increase in the continuous  $a(t)$ :

$$a(t) \rightarrow 10a(t) \approx 10(4t)^{2/3}. \quad (74)$$

For  $X_k$  (in the  $k = 4m$  mode), we find a modest decline of  $\sim 0.03$  in the root mean square, due to the order-of-magnitude increase in the scale factor. Figure 14 shows  $\log n_k$  for both forms of the scale factor for 10 oscillations following the end of broad resonance. The decrease in  $\log n_k$  because of the effect of the larger scale factor causes a reduction of just  $\sim 0.002$  in the root mean square of the occupation number  $n_k$  at 10 oscillations after broad resonance terminates.

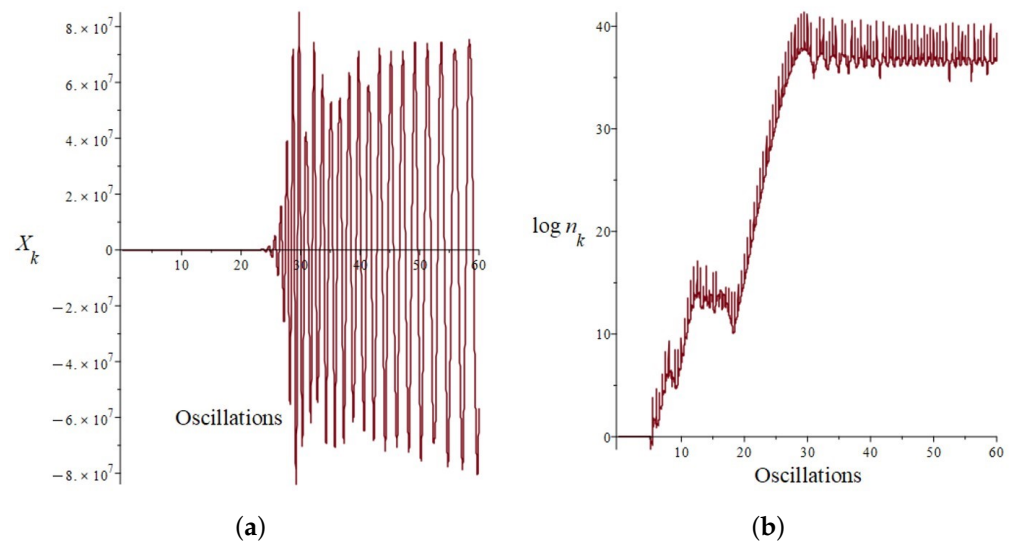


**Figure 13.** (a) The scalar field and (b) occupation number for the first 60 oscillations in a model with the smooth scale factor. The graphs show reduced values of  $X_k$  and  $\log n_k$  compared to Figure 12 because of the effect of the order-of-magnitude increase in  $a(t)$ .

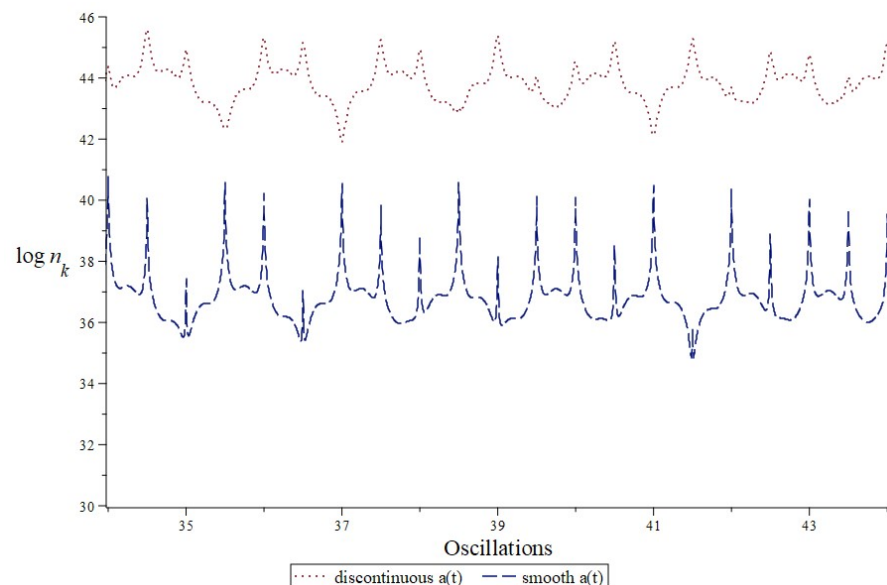


**Figure 14.** These plots compare 10 oscillations of  $\log n_k$  after the end of broad resonance at  $\sim 34$  oscillations for the two functional forms of the scale factor.

Local maxima in  $\log n_k$  for the smooth scale factor in Figure 14 occur at every half oscillation of  $\phi$  at  $t = \frac{1}{2}, 1, \frac{3}{2}, \dots$ . At these points, where  $\sin(2\pi t) = 0$  in Equation (72), the frequency reduces to

$$\omega_k = 2\pi \frac{k}{a}, \quad (75)$$

with values of less than one:  $0.080 \lesssim \omega_k \lesssim 0.095$ . For the 10 oscillation periods under consideration with the smooth scale factor model, this range of fractional frequencies has the effect of increasing the contribution of the term containing the kinetic energy  $\dot{X}_k$  in the occupation number:

$$n_k = \frac{\omega_k}{2} \left( \frac{|\dot{X}_k|^2}{\omega_k^2} + |X_k|^2 \right) - n_{k0}, \quad (76)$$

even as it tends to suppress the contribution of the potential-like  $X_k$  term. Thus, the small fractional frequency generates the local maxima. The range of larger frequencies with the cusped scale factor following the end of resonance,  $0.80 \lesssim \omega_k \lesssim 0.95$ , has less of an effect and intersperses some local minima, depending on the relative values of  $\dot{X}_k$  and  $X_k$  at the half-oscillation times.

We are able to provide some understanding of the differences in appearance of  $\log n_k$ —that is, the greater degree of dispersion of the amplitudes above the average occupation number in Figure 13b in comparison with Figure 12b—by examining in detail the effect of the fractional frequency. At oscillation 36, for example, the occupation numbers  $\log n_k(36)$  are approximately 45.3 and 40.2 for the cusped and smooth scale factor models, respectively. The kinetic term in the energy, amplified by the frequency, for the most part determines the occupation number in both models. The average occupation numbers over four oscillations from oscillation 34 to 38 are approximately 43.9 and 36.8, respectively—yielding an increase during this period of  $\sim 0.03$  with the cusped scale factor and  $\sim 0.09$  with the smooth model. The lower level of the scalar field in the smooth model and (more importantly) its time derivative moderate what would otherwise be an approximately 10-fold difference in the increases based on the values of  $\omega_k$  alone. Thus, we see the greater dispersion of amplitudes above the average  $\log n_k$  in Figure 13. Appendix E contains a table that lists some of the supporting data associated with the behavior around oscillation 36 and related graphs.

## 7.2. Number Density

The number density of the scalar field quanta has its basis in the process of broad parametric resonance KLS characterize in their paper as *stochastic*—that is, random. They show that the variation in the phase  $\theta_k$  of the scalar field  $\chi$  in the course of semiclassical interactions between the  $\chi$ -particles and the oscillating inflaton field is very much greater than  $\pi$ , which makes successive phases effectively random. However, this does not mean that there is no net energy flow from one sector to the other. In fact, a growth in the number of particles between classical scattering events can be as much as three times as probable as a decrease, based on the numerical effect of possible values for the phase angle in the recurrence relation governing resonance. KLS also separate preheating into two time periods. The first period precedes all backreaction and rescattering, and the second period involves the effect of those interactions on the number density, which can be significant. Backreaction and rescattering are quantum effects in which the created  $\chi$ -particles interact with the background inflaton field. In backreaction, interactions can alter the effective masses of the particles and the frequency of the inflaton oscillations. Rescattering involves a created particle scattering again, either off an inflaton or another  $\chi$ -particle. However, KLS conclude that the duration of the second period is so brief that, during it, they can safely neglect the expansion of the universe, and their analysis of that part does not depend on the scale factor. Therefore, here, we shall determine the effect of the continuous scale factor on the number density conversely without including backreaction and rescattering.

Semiclassical scattering leading to quantum-mechanical  $\chi$ -particle production involves the interaction of the scalar field  $\chi$  and the background inflaton field oscillating around zero. KLS derive the number density of the  $\chi$  field from the adiabatic approximation solution to Equation (66):

$$X_k(t) = \frac{\alpha_k(t)}{\sqrt{\omega_k}} e^{-i \int^{t_j} dt \omega_k} + \frac{\beta_k(t)}{\sqrt{\omega_k}} e^{+i \int^{t_j} dt \omega_k}, \quad (77)$$

with the scalar field phase  $\theta_k^j = \int^{t_j} dt \omega_k$  and  $t_j$  representing the time at the end of the  $j^{\text{th}}$  oscillation—such that as time  $t \rightarrow t_j$ , the inflaton field is oscillating around its minimum,  $\phi \rightarrow 0$ . The functions  $\alpha_k(t)$  and  $\beta_k(t)$  are time-dependent Bogoliubov transformation coefficients [34].

Around  $\phi \approx 0$ , Equation (66) becomes

$$\ddot{X}_k + \left[ \frac{k^2}{a^2} + g^2 \Phi^2(t) m^2 (t - t_j)^2 \right] X_k = 0. \quad (78)$$

The scalar field  $\chi$  with an effectively random phase  $\theta_k^j$  completes a half-oscillation at time  $t \rightarrow t_j$  for  $j = 1, 2, 3, \dots$ . As  $t \rightarrow t_j$  for each half-oscillation of  $\chi$ , the inflaton field concurrently oscillates near zero, creating a period of nonadiabatic energy transfer, which leads to exponential growth in the number of  $\chi$ -quanta according to Equation (69). At other times, the number density  $n_\chi$  remains stable. Introduction of parameters

$$\tau = k_*(t - t_j) \text{ and } \kappa = \frac{k}{ak_*} \quad (79)$$

recasts Equation (78) as a differential equation with a parabolic cylinder function solution:

$$\frac{d^2 X_k}{d\tau^2} + (\kappa^2 + \tau^2) X_k = 0, \quad (80)$$

which is also the Schrödinger equation with an unstable quadratic potential,  $V(\phi) \propto -\tau^2$ . Appendix F derives the largest mode to participate in the broad parametric resonance,  $k_* = \sqrt{gm\Phi}$ . The scattering of solutions  $X_k$  of Equation (66) leads to a recurrence relation for the Bogoliubov coefficients, which may be represented by transfer matrix

$$\begin{pmatrix} \alpha_k^{j+1} e^{-i\theta_k^j} \\ \beta_k^{j+1} e^{+i\theta_k^j} \end{pmatrix} = \begin{pmatrix} \frac{1}{D_k} & \frac{R_k^*}{D_k} \\ \frac{R_k}{D_k} & \frac{1}{D_k^*} \end{pmatrix} \begin{pmatrix} \alpha_k^j e^{-i\theta_k^j} \\ \beta_k^j e^{+i\theta_k^j} \end{pmatrix}. \quad (81)$$

KLS provide the reflection  $R_k$  and transmission  $D_k$  amplitudes from the solutions of the parabolic cylinder equation and also the phase angle  $\varphi_k$ , which is a complicated function of the parameter  $\kappa$ :

$$\varphi_k = \arg \Gamma \left( \frac{1 + i\kappa^2}{2} \right) + \frac{\kappa^2}{2} \left( 1 + \log \frac{2}{\kappa^2} \right). \quad (82)$$

With these, the recurrence relation becomes

$$\begin{pmatrix} \alpha_k^{j+1} \\ \beta_k^{j+1} \end{pmatrix} = \begin{pmatrix} \sqrt{1 + e^{-\pi\kappa^2}} e^{i\pi\varphi_k} & i e^{-i\frac{\pi}{2}\kappa^2 + 2i\theta_k^j} \\ -i e^{-i\frac{\pi}{2}\kappa^2 - 2i\theta_k^j} & \sqrt{1 + e^{-\pi\kappa^2}} e^{-i\pi\varphi_k} \end{pmatrix} \begin{pmatrix} \alpha_k^j \\ \beta_k^j \end{pmatrix}. \quad (83)$$

Note that the occupation number  $n_k$  in Equation (71) just depends on the Bogoliubov coefficient  $\beta_k$  [35]:

$$n_k = |\beta_k|^2, \quad (84)$$

and that for a coherent process  $n_k \gg 1$ , it leads to the recurrence relation

$$n_k^{j+1} \approx \left[ 1 + 2e^{-\pi\kappa^2} - 2 \sin(\theta_{\text{tot}}^j) e^{-\frac{\pi}{2}\kappa^2} \sqrt{1 + e^{-\pi\kappa^2}} \right] n_k^j, \quad (85)$$

with the accumulated phase

$$\theta_{\text{tot}}^j = 2\theta_k^j - \varphi_k + \arg \beta_k^j - \arg \alpha_k^j. \quad (86)$$

Because the variation in the phases  $\theta_k^j$  is very much greater than  $\pi$ , the randomness of  $\theta_k^j$ —and by extension the randomness of  $\alpha_k^j$  and  $\beta_k^j$  as functions of  $\theta_k^j$ —make  $\theta_{\text{tot}}^j$  stochastic. Noting that resonance begins to be suppressed unless  $\pi\kappa^2 \lesssim 1$ , KLS found that, for  $\pi\kappa^2 \ll 1$ , a growth in the number of particles is three times as likely as a decrease. Within the range  $0 < \theta_{\text{tot}}^j \leq 2\pi$ , values of  $0 < \theta_{\text{tot}}^j < \frac{\pi}{4}$  and  $\frac{3\pi}{4} < \theta_{\text{tot}}^j \leq 2\pi$  cause an increase in the number of particles according to Equation (85); only over one quarter of the possible range of phases,  $\frac{\pi}{4} < \theta_{\text{tot}}^j \leq \frac{3\pi}{4}$ , does the number of  $\chi$ -particles decrease, as energy flows (incoherently) back to the inflaton field. A second recurrence relation also obtainable [32] from the Mathieu Equation (67):

$$n_k^{j+1} = n_k^j e^{2\pi\mu_k^j}, \quad (87)$$

in combination with Equation (85), yields the Floquet characteristic exponent

$$\mu_k^j = \frac{1}{2\pi} \log \left[ 1 + 2e^{-\pi\kappa^2} - 2 \sin(\theta_{\text{tot}}^j) e^{-\frac{\pi}{2}\kappa^2} \sqrt{1 + e^{-\pi\kappa^2}} \right]. \quad (88)$$

Integration of  $n_k$  for all modes that participate in broad parametric resonance gives rise to the total number density of  $\chi$ -quanta:

$$n_\chi = \frac{1}{(2\pi a)^3} \int d^3k n_k(t) = \frac{1}{4\pi^2 a^3} \int dk k^2 e^{2\mu_k m t}. \quad (89)$$

The units of number density  $n_\chi$  are the expected  $\text{m}^{-3}$ , since occupation number  $n_k(t)$  is dimensionless. KLS evaluate the integral on the far-right-hand side of Equation (89) by the steepest descent method and estimate the number density to be

$$n_\chi \approx \frac{k_*^3}{64\pi^2 a^3 \sqrt{\pi\mu m t}} e^{2\mu m t}. \quad (90)$$

They also determine the maximum Floquet characteristic exponent  $\mu$  associated with an unknown maximum  $k_{\text{max}}$ , estimated as  $k_{\text{max}} \approx \frac{k_*}{2}$ .

We use the proportionality

$$n_\chi \propto \frac{1}{a^3 \sqrt{\mu m t}} e^{2\mu m t} \quad (91)$$

to perform a numerical analysis of the effect of the continuous scale factor by examining the ratio

$$R_\chi = \frac{n_{\chi a(t)\text{smooth}}}{n_{\chi a(t)\text{cusp}}}. \quad (92)$$

The terms  $n_{\chi a(t)\text{smooth}}$  and  $n_{\chi a(t)\text{cusp}}$  represent the number densities of the smooth and cusped scale factor models, respectively. We anticipate a decrease in the number density due to the increase in volume, moderated to a certain amount by the dependence of the proportionality in Equation (91) on  $\mu$ . The use of the proportionality eliminates the dependence on the unknown mode  $k_*$ , which KLS estimate as  $k_*(t) \approx \sqrt{gm\Phi(t)}$ , as detailed in Appendix F.

In the absence of  $\frac{e^{2\mu m t}}{\sqrt{\mu m t}}$ , the greater time allowed for the expansion of space in the smooth model would on its own cause dilution—that is, a decrease in the number density. The order-of-magnitude increase in the smooth scale factor alone would reduce the number density by the cube of the scale factor increase:  $\sim 10^{-3}$ . However, the effect of the broad parametric resonance in preheating—in particular, the term  $\frac{e^{2\mu m t}}{\sqrt{\mu m t}} > 1$ —may modestly

offset the mere increase in the volume of space. The extent of the offset is dependent on the stochastic  $\sin(\theta_{\text{tot}}^j)$  in Equation (88). Figure 15 displays the ratio  $R_\chi$  of number density of the smooth scale factor to the discontinuous scale factor as a function of time (again expressed as the number of oscillations). The value of the ratio at the start of preheating,  $\sim 10^{-3}$ , reflects the effect only of the expansion of space. As preheating progresses, however,  $R_\chi$  rises to a level slightly greater than  $1.7 \times 10^{-3}$  at the end of broad parametric resonance, at around 34 oscillations, in the limiting case in which  $\sin(\theta_{\text{tot}}^j)$  is consistently equal to  $-1$ . In contrast, as  $\sin(\theta_{\text{tot}}^j)$  increases toward 1,  $R_\chi$  decreases. For example, at  $\sin(\theta_{\text{tot}}^j) = 0$ ,  $R_\chi \sim 1.6 \times 10^{-3}$ , and  $R_\chi$  is about  $1.3 \times 10^{-3}$  at  $\sin(\theta_{\text{tot}}^j) = 0.65$ . With a slightly larger stochastic value,  $n_{\chi a(t)\text{cusp}}$  is not directly calculable via this method at lower oscillations, and with a stochastic phase of 0.8, the calculations of both  $n_{\chi a(t)\text{cusp}}$  and  $n_{\chi a(t)\text{smooth}}$ , even at the end of 34 oscillations, because that would require the Floquet index  $\mu$  in Equation (88) to be negative. The negative Floquet index signals an essentially unphysical solution, which the model formalism does not support; physically, this scenario would describe a net energy flowing back into the inflaton field, while mathematically, the formalism breaks down because the saddle point integration method is no longer usable. Thus, examination of the ratio  $R_\chi$  places a bound on the effect of the continuous scale factor. The reduction of the number density due to the expansion of space alone,  $\sim 10^{-3}$ , increases only slightly, by, at most, about  $1.7 \times 10^{-3}$  after preheating, depending on the values of the stochastic  $\sin(\theta_{\text{tot}}^j)$  angles.

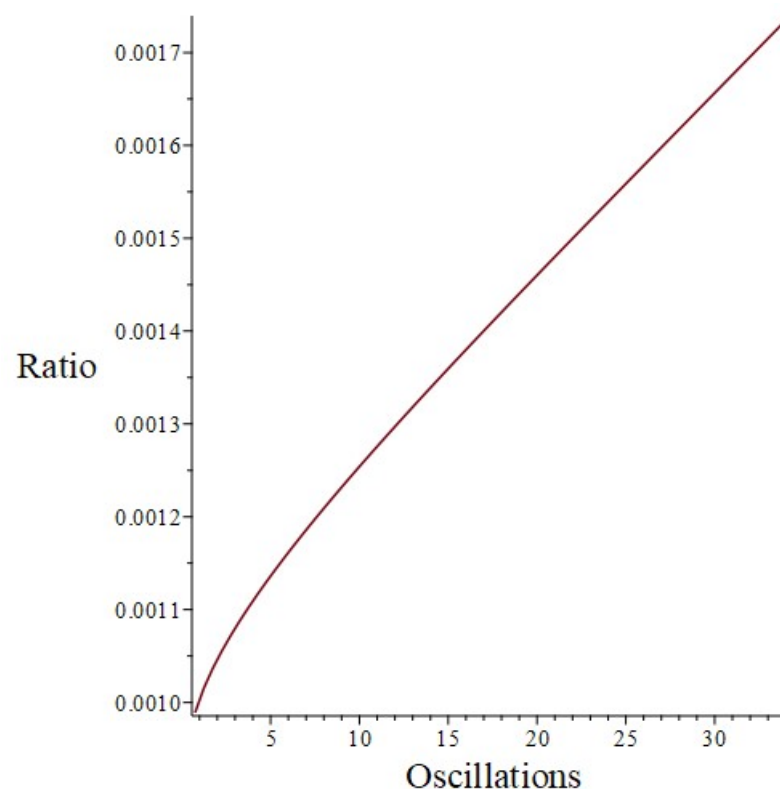


**Figure 15.** The ratio  $R_\chi$  of  $n_\chi$  for the smooth scale factor, to that with  $a(t)$  with a discontinuous derivative at the end of inflation, as used by KLS. The increase in volume in the smooth model, resulting from the extra time given for space to expand as inflation tails off, dilutes  $n_\chi$  by  $\sim 10^{-3}$ , which the broad parametric resonance term  $e^{2\mu mt} / \sqrt{\mu mt}$  partially tends to offset. Maximizing the offset with the total phase  $\sin(\theta_{\text{tot}}^j) = -1$  in Equation (88) minimizes the dilution, and that is what is shown in this figure. Thus, with the smooth scale factor,  $n_\chi$  should be diluted by at least the ratios shown here.

## 8. Conclusions

This work has explored the consequences of applying the reasonable expectation of smoothness to the physical expansion of space, as expressed by the characteristic scale factors defining the early universe evolving through its generally accepted, broadly defined epochs. We focused on the nearly instantaneous slice of time separating the inflationary era and the subsequent era in which the stress–energy tensor was assumed to be dominated by a single component: either radiation or matter. We focused on the transition out of inflation specifically because it is where we inevitably expect to find the sharpest change in the behavior of the scale factor; assuming some realistic values for primordial parameters reveals that the time derivative of the scale factor can decrease by a factor of  $\frac{1}{120}$  between inflation and the radiation era. Rather than being guided by a specific equation-of-state model, we imposed a first-derivative smoothness requirement upon the scale factor and looked at phenomenological interpolating functions that could connect the inflation and subsequent eras. The assumption of a continuously, steadily declining (but not contracting) slope after the end of inflation led to an in-depth examination of families of interpolating candidates with shifted power-law dependencies on time. We imposed the same requirements of smoothness at the beginning and at the end of the brief interpolating transition period.

From these matching conditions, we uncovered that it was necessary to place the vertices of power-law interpolating functions with indices  $n < 1$  prior to the end of inflation at  $t_f$  and the vertices of functions with  $n > 1$  subsequent to  $t_f$ , with the displacement in either case parameterized by  $\delta$ . Also, the transition period  $\Delta$ —the duration of the period between the end of inflation and the single-component universe (whether modeled as composed of radiation or matter)—was initially unknown. However, a remaining uncertainty in the parameters of the model was implicit in our transition model. We could not find specific expressions for all of them without imposing additional conditions, and we could do no better than finally expressing the displacement  $\delta$  in terms of the transition period  $\Delta$ . Graphical analysis of the Hubble parameter and the equation-of-state and speed-of-sound stability and causality constraints allowed us to identify physically reasonable interpolating power-law functions as those with indices that approached the power-law indices  $\frac{1}{2}$  and  $\frac{2}{3}$  for radiation and matter single-component universes, respectively. Numerical analyses demonstrate the remarkable result that the actual transition lasts approximately  $10^{-37}$  s, essentially regardless of the composition of the single-component universe that follows the transition and the duration  $\Delta$ . In addition, the universe enters the single-component era about an order of magnitude (or approximately 2–3  $e$ -folds) larger than it would have been if subject to a scale factor with a discontinuous slope, which switched instantaneously to  $t^{1/2}$  or  $t^{2/3}$  behavior at the end of the inflationary epoch. Although the form of the interpolating function is not exponential, the increase in the lifespan of the universe,  $10^{-37}$  s, is not inconsequential compared to the assumption for the inflationary expansion of the universe:  $N \approx 60$   $e$ -folds. We understand the outcome to be a universe given an additional short sliver of time in which to grow larger simply because we imposed a condition of smoothness on the physical expansion of space. The numerical analysis adds precision to this result. For a radiation-dominated era following the transition, at  $10^{-37}$  s, the increase in the size of the universe attained 98.5% of its asymptotic value, and the corresponding figure for a subsequent matter-dominated era is 98.3%. Generalizing the approach, using a multiple-component universe would also be interesting, as would considering the high-scale physics of inflation that might provide the friction needed to end inflation in a smoother way, or evaluating how the changed size of the postinflationary universe could affect later inflation-related observables, such as the distribution of galaxies or the temperature and polarization structure of the CMB.

We proceeded to examine the effect of the theoretical changes we had described to the dynamic expansion of space (characterized by a smooth scale factor and the resulting predicted increase in the size of the universe) on a subsequent preheating era. The evolution of the universe after inflation remains highly speculative because of the challenges implicit in experimental confirmation. A period of reheating appears to be required in order to

be consistent with the later stages of cosmological development, but the details of the reheating dynamics can depend sensitively on the nature of the particle species available to be excited—including as-yet unobserved high-mass species that may not be accessible at standard model scales but could nonetheless have been active participants in the dynamics of the hot, dense early universe. However, we also discussed the intricate, highly technical theory of preheating developed by Kofman, Linde, and Starobinsky to address some generic problems with reheating. We applied the KLS formalism to our model with a smooth interpolating scale factor leading into a matter-dominated universe, in order to gauge the effects of the smoothing on the most sensitive  $\chi$ -particle occupation number  $n_k$  and the corresponding number density  $n_\chi$ . We were able to estimate the numerical changes compared with the results obtained using the standard cusped scale factor, and we concluded that the differences are not necessarily numerically significant, apart from a dilution in the total particle density that should be common to all models that predict somewhat larger universes after the end of inflation. Specifically, for the occupation number of the most aggressively growing  $\chi$  mode, we found a modest decline in  $\log n_{k=4m}$  of  $\sim 2 \times 10^{-3}$  in the root mean square for 10 oscillations following the end of broad parametric resonance, which is a consequence of a decrease of just  $\sim 3 \times 10^{-2}$  in the root mean square of the scalar field  $\chi_k$  over the same period. In addition, by constructing a relation consisting of the ratio of the number density in the cosmology with the smooth scale factor to that with the cusped scale factor, we determined a partial offset to the expected dilution of the quantity of bosons produced by broad parametric resonance due to the approximate  $10^3$  increase in the unit volume of space caused by the larger smooth scale factor. The stochastic nature of broad parametric resonance precludes a specific prediction, but we found an additional modest increase in the proportion, with an upper bound of  $\lesssim 1.7 \times 10^{-3}$ .

It may be somewhat surprising that the effect of a proposed smoothing of the scale factor is so minor—mostly limited to the natural rarefaction of the  $\chi$  particles that comes with a spatially larger universe. Regarding the possibility (in a case of optimal phase alignment) of, at most, an additional near doubling per unit volume of the number density, we noted that a doubling of a small number of something in a unit volume may easily be thought of as not negligible. However, in terms of the many, many orders of magnitude of primal particles in a unit volume of early space, we consider the outcome of having, at most, close to twice as many as not being of substance. Thus, we view the result of the numerical analysis of the effect of a not insignificant increase in the size of the universe to represent confirmation of the comparative invariance of the KLS preheating model to these kinds of modifications. We are satisfied that our result represents a modestly useful contribution to the body of work in support of this iconic theory.

**Author Contributions:** Conceptualization, H.O. and B.A.; Methodology, H.O. and B.A.; Investigation, H.O. and B.A.; Writing—original draft, H.O.; Writing—review and editing, B.A. All authors have read and agreed to the published version of the manuscript.

**Funding:** This research received no external funding.

**Data Availability Statement:** Computational data is available from the authors by request.

**Conflicts of Interest:** The authors declare no conflict of interest.

## Appendix A

In this appendix, we review the derivation of the inverse relation between the radiation temperature of the universe and the scale factor, following the approach outlined by Ryden [1]. In an isothermal environment, the first law of thermodynamics

$$dQ = dE + p dV \quad (\text{A1})$$

reduces to

$$\frac{dE}{dt} = -p \frac{dV}{dt}. \quad (\text{A2})$$

After substituting the pressure of a relativistic gas,  $p_\gamma = \frac{\rho_\gamma}{3}$ , and the CMB black body energy density,  $\rho_\gamma = 4\sigma T^4$ , we obtain

$$\frac{d(\rho_\gamma V)}{dt} = -\frac{\rho_\gamma}{3} \frac{dV}{dt}, \quad (\text{A3})$$

$$\frac{d\rho_\gamma}{dt} V + \rho_\gamma \frac{dV}{dt} = -\frac{\rho_\gamma}{3} \frac{dV}{dt}, \quad (\text{A4})$$

$$\frac{1}{T} \frac{dT}{dt} = -\frac{1}{3V} \frac{dV}{dt}. \quad (\text{A5})$$

In an expanding universe with volume element  $V = a^3(t)L^3$ , the relation becomes

$$\frac{1}{T} \frac{dT}{dt} = -\frac{1}{3a^3(t)L^3} \frac{d[a^3(t)L^3]}{dt} = -\frac{1}{a} \frac{da}{dt}, \quad (\text{A6})$$

which is an elementary separable differential equation, satisfied for

$$T \propto a^{-1}. \quad (\text{A7})$$

## Appendix B

This appendix details the derivation of the working forms of the equation of state in flat space, defined as

$$\epsilon_H = -\frac{\dot{H}}{H^2} = -\frac{\ddot{a}/a - (\dot{a}/a)^2}{(\dot{a}/a)^2} = 1 - \frac{\ddot{a}/a}{(\dot{a}/a)^2}. \quad (\text{A8})$$

Substituting the first Friedmann equation in flat space:

$$H^2(t) = \left(\frac{\dot{a}}{a}\right)^2 = \frac{8\pi G}{3}\rho, \quad (\text{A9})$$

and the acceleration equation:

$$\frac{\ddot{a}}{a} = -\frac{4\pi G}{3}(\rho + 3p), \quad (\text{A10})$$

gives

$$\epsilon_H = 1 - \frac{-\frac{4\pi G}{3}(\rho + 3p)}{\frac{8\pi G}{3}\rho} = \frac{3}{2}(1 + \omega), \quad (\text{A11})$$

where  $\omega$  would be the coefficient of proportionality between pressure  $p$  and density  $\rho$  in a single-component universe. For an exponential scale factor  $a = e^{Ht}$ , we clearly have  $d \log a = H dt$ , but, in fact, this relationship holds more generally, as integrating it just gives the definition of  $H$ . Thus, we can alternatively express  $\epsilon_H$  as

$$\epsilon_H = -\frac{\dot{H}}{H^2} = \frac{1}{H} \left( -\frac{\dot{H}}{H} \right) = \frac{1}{H} \frac{d}{dt} \log(H^{-1}) = \frac{d \log(H^{-1})}{d \log a}, \quad (\text{A12})$$

that is, as the slope along a plot of  $\log(H^{-1}) = -\log H$  versus  $\log a$ .

### Appendix C

The derivation of  $\epsilon_{H \text{ expected}} = \frac{1}{n}$  for a single-component universe is:

$$a_n(t) = a_n(t_0) \left( \frac{t}{t_0} \right)^n \tag{A13}$$

$$\dot{a}_n(t) = n \frac{a_n(t_0)}{t_0^n} t^{(n-1)} = \frac{n}{t} a_n(t) \tag{A14}$$

$$\ddot{a}_n(t) = n \frac{a_n(t_0)}{t_0^n} (n-1) t^{(n-2)} = \frac{n-1}{t} \dot{a}_n(t). \tag{A15}$$

Therefore,

$$\epsilon_H = -\frac{\dot{H}}{H^2} = 1 - \frac{\ddot{a}/a}{(\dot{a}/a)^2} = 1 - \frac{a_n(t)\ddot{a}_n(t)}{\dot{a}_n(t)^2} \tag{A16}$$

$$= 1 - \frac{a_n(t) \frac{n-1}{t} \dot{a}_n(t)}{\dot{a}_n(t)^2} = 1 - \frac{a_n(t) \frac{n-1}{t}}{\dot{a}_n(t)} = \frac{1}{n}. \tag{A17}$$

### Appendix D

We reproduce here the well-known stability–instability chart [32,33] showing the regions of the parameter space in which the initial value problem solutions for the Mathieu Equation (67) are either stable or unstable.

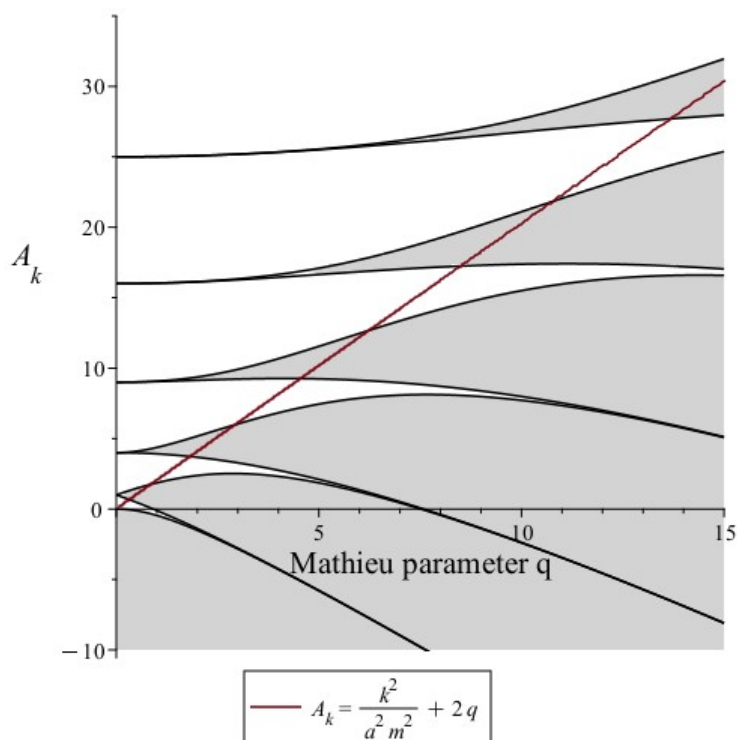


**Figure A1.** Stability–instability chart. The areas highlighted in gray are the regions of instability in the  $q$ - $A_k$  parameter space. The plot also depicts the Mathieu equation parameters associated with the equation of motion solutions. Note that  $q$  and  $A_k$  decrease as time progresses.

The regions of instability correspond to the periods of sustained exponential growth in  $n_k$  during preheating. Figure A2 superimposes the Mathieu equation instability regions associated with the equation of motion in the KLS model on the time evolution of  $\log n_k$ , to highlight this correspondence.

There are some interesting and noteworthy differences between the behavior in the three broad-resonance growth regions for  $n_k$  (at least for the particular, rapidly growing value  $k = 4m$  we selected). There are small oscillations visible, in addition to the secular growth in  $\log n_k$ . During periods when the parameters make the Mathieu equation stable (the white bands in Figure A2), the oscillations are comparatively chaotic; this is also what is seen in Figure 14 after the last resonant growth period has ended. There is a certain amount of approximately periodic behavior, due to being driven by the amplitude squared of the inflaton field, so there are fairly stark features every half an inflaton oscillation period. However, underneath these is a chaotically varying baseline. During the periods of resonance (the gray bands), the baseline behavior is different, with approximately exponential growth in the occupation number, as is typical in an unstable driven system. On top of this are additional oscillations, qualitatively similar in some ways to those in the stability regions. However, there are also clear manifestations of the nonlinearity of the Mathieu equation, in the form of period doubling or tripling. When the exponential growth is subtracted, the residual still has, on average, one peak per half oscillation of the inflaton field. However, these peaks are not evenly placed or of equal amplitude. During the second shown resonance region, the oscillating residuals have periods equal to the full inflaton oscillation period—a period doubling phenomenon. Within each full oscillation are two dissimilar up-and-down cycles. Moreover, in the vicinity of and during the first, shortest resonant period, there is period tripling, with the periodic residuals taking one and half inflaton oscillation cycles to return fully to their original phase space positions.

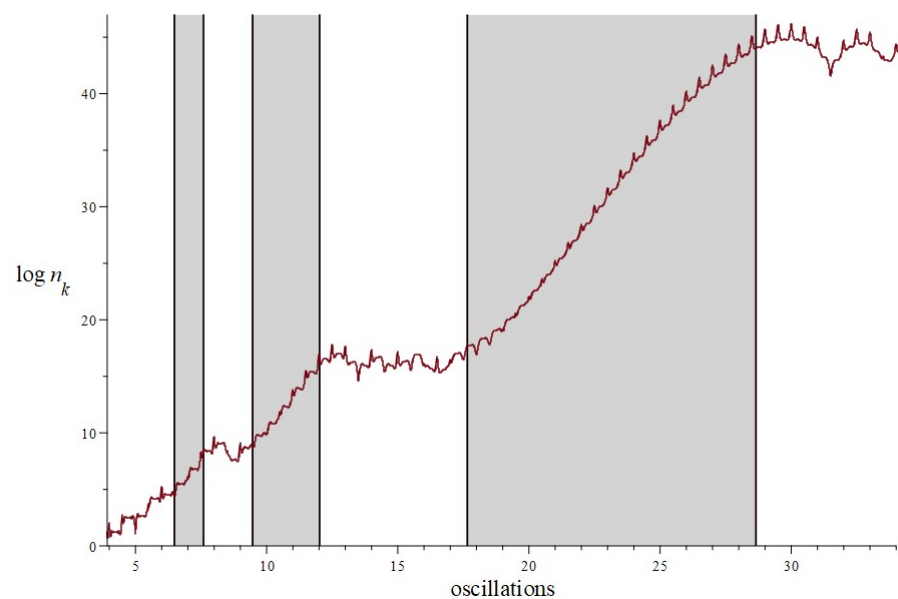


**Figure A2.** The final three instability regions superimposed on the  $\log n_k$  resonance growth. As the number of oscillations increases, we see exponential growth in the occupation number as the  $q$  and  $A_k$  of Figure A1 decline toward zero and the equation of motion crosses the last three instability regions.

## Appendix E

Below, Figures A3 and A4 show the behavior of the scalar field  $X$  and its time derivative in the two models. Table A1 also lists some of the supporting data associated with the behavior of the scalar field around oscillation 36.

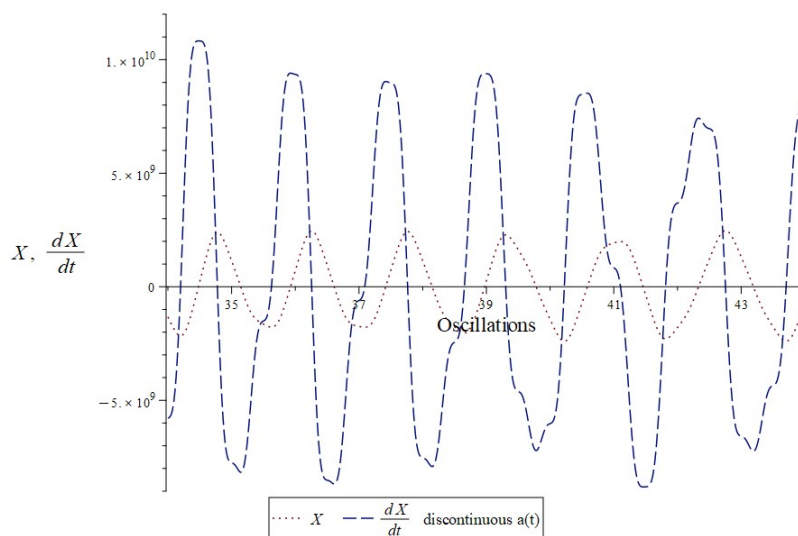


**Figure A3.** Plots of scalar field  $X$  and its time derivative  $\dot{X}$  with the cusped scale factor for 10 oscillations following the end of broad parametric resonance.

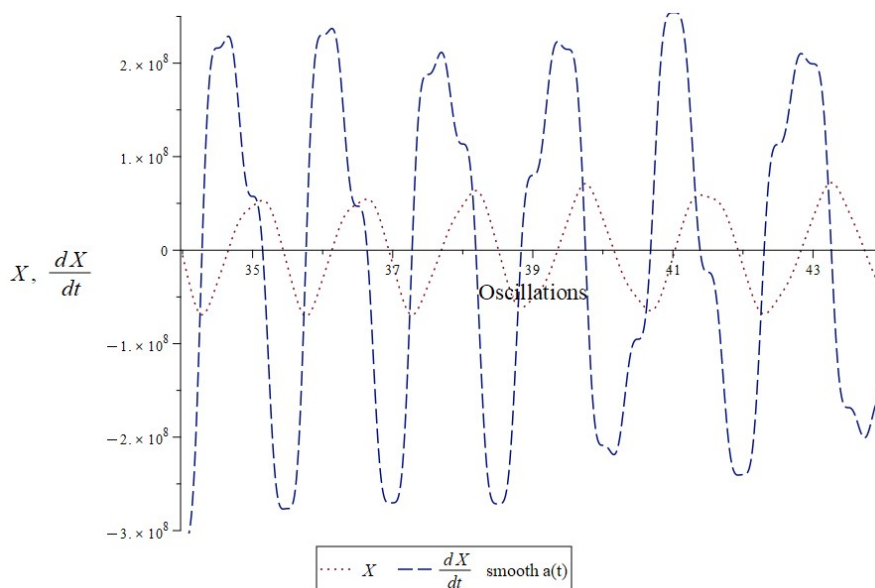


**Figure A4.** Plots of scalar field  $X$  and its time derivative  $\dot{X}$  with the smooth scale factor for 10 oscillations following the end of broad parametric resonance.

**Table A1.** Data in support of the differences in appearance between Figures 12b and 13b. The last column represents the increase in occupation number  $\log n_k(36)$  compared to the average value over 4 oscillations from oscillation 34 to 38, which are 43.9 and 36.8 for the KLS and smooth scale factor models, respectively.

$a(t)$ Model	$\omega_k$	$\omega_k  X ^2$	$\frac{ \dot{X} ^2}{\omega_k}$	$\log n_k(36)$	Increase
cusped	0.91	$4.62 \times 10^{17}$	$9.56 \times 10^{19}$	45.3	0.03
smooth	0.091	$8.71 \times 10^{13}$	$5.79 \times 10^{17}$	40.2	0.09

**Appendix F**

Appendix F details the derivation of the range of modes  $k_*$  that participate in the broad parametric resonance process. KLS provide the typical frequency for the scalar

field  $\chi$  oscillations,  $\omega(t) = \sqrt{k^2 + g^2\phi^2(t)}$ , subject to the adiabatic instability condition, Equation (69):

$$\frac{\dot{\omega}}{\omega^2} \gtrsim 1 \quad (\text{A18})$$

$$\frac{\dot{\omega}}{\omega^2} = \frac{g^2\phi\dot{\phi}}{(k^2 + g^2\phi^2)^{3/2}} \gtrsim 1. \quad (\text{A19})$$

The instability condition yields the inequality defining the unstable modes. The inflaton at the end of inflation is an oscillating field of the form  $\phi(t) = \Phi(t) \sin(mt)$ . For broad resonance, when  $\phi(t)$  is small and the decaying envelope  $\Psi$  is approximately constant over the period of a single oscillation,  $\dot{\phi} \approx m\Phi$ . This makes the resonance condition

$$1 \lesssim \frac{g^2\phi m\Phi}{(k^2 + g^2\phi^2)^{3/2}} \quad (\text{A20})$$

$$k^2 \lesssim (g^2\phi m\Phi)^{2/3} - g^2\phi^2. \quad (\text{A21})$$

We find the maximum range of  $k$  by taking the derivative of the inequality (A21) to maximize the inflaton value  $\phi_*$ :

$$\frac{2g^{4/3}m^{2/3}\Phi^{2/3}}{3\phi_*^{1/3}} - 2g^2\phi_* = 0, \quad (\text{A22})$$

for which the solution is

$$\phi_* = (3)^{-3/4} \sqrt{\frac{m\Phi}{g}} \approx \frac{1}{2} \sqrt{\frac{m\Phi}{g}}. \quad (\text{A23})$$

Substituting  $\phi_* \approx \frac{1}{2} \sqrt{\frac{m\Phi}{g}}$  into  $k_{\max}^2 \lesssim (g^2\phi_* m\Phi)^{2/3} - g^2\phi_*^2$ , we find

$$k_{\max} \lesssim \sqrt{\frac{gm\Phi}{2}}. \quad (\text{A24})$$

Taking  $k \rightarrow 0$  in Equation (A20) generates an expression for the inflaton associated with the minimum-range of mode  $k$ :

$$\frac{g^2\phi m\Phi}{(g^2\phi^2)^{3/2}} \gtrsim 1 \quad (\text{A25})$$

$$\phi \lesssim \sqrt{\frac{m\Phi}{g}}. \quad (\text{A26})$$

Figure A5 shows a standard graphical representation of the bands of  $\phi(t)$  associated with the minimum and maximum ranges of  $k$ . We note that  $k_{\max}^2$  applies to a band of  $\phi(t)$  for which  $|\phi| \leq 2\phi_*$ . Thus, we find

$$k_* = \sqrt{gm\Phi}. \quad (\text{A27})$$

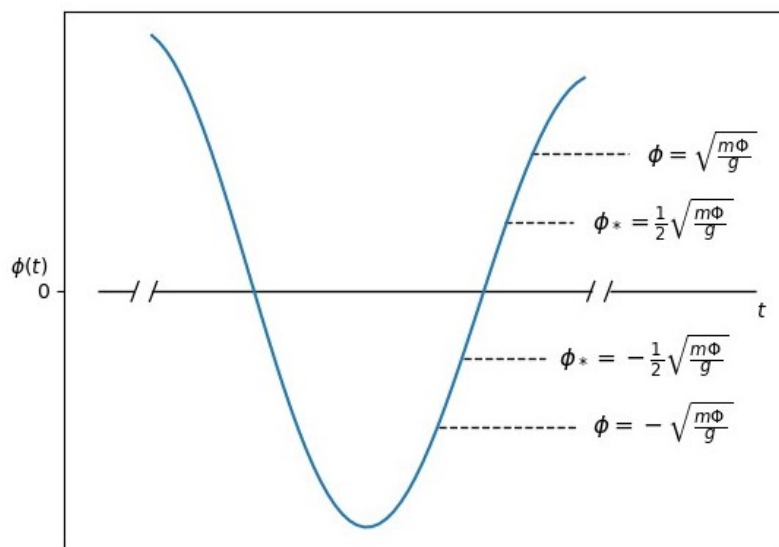


**Figure A5.** The outer and inner pairs of dotted lines represent the ranges of  $\phi(t)$  that participate in parametric resonance. The wider outer band corresponds to the values of  $\phi(t)$  that participate in the resonance for the minimal Fourier component—that is, as  $k \rightarrow 0$ . The inner band,  $-\frac{1}{2}\sqrt{m\Phi/g} \leq \phi_* \leq \frac{1}{2}\sqrt{m\Phi/g}$ , corresponds to the participating  $\phi(t)$  associated for the modes with  $k_* = \sqrt{gm\Phi}$ . This is the preheating band of broad parametric resonance. Explosive growth in the number of particles occurs as  $\phi(t) \rightarrow 0$ .

## References

- Ryden, B. *Introduction to Cosmology*; Addison Wesley: San Francisco, CA, USA, 2003.
- Liddle, A.R.; Lyth, D.H. *Cosmological Inflation and Large-Scale Structure*; Cambridge University Press: New York, NY, USA, 2006.
- Linde, A.D. The Inflationary Universe. *Rep. Prog. Phys.* **1984**, *47*, 925. [CrossRef]
- Baumann, D. TASI Lectures on Inflation. *arXiv* **2009**, arXiv:0907.5424.
- Lesgourgues, J. Inflationary Cosmology. Lecture Notes. Available online: <https://lesgourg.github.io/courses.html> (accessed on 22 March 2022).
- Liddle, A.R. *An Introduction to Modern Cosmology*; Wiley & Sons: West Sussex, UK, 2015.
- Bassett, B.A.; Tsujikawa, S.; Wands, D. Inflation Dynamics and Reheating. *Rev. Mod. Phys.* **2006**, *78*, 537. [CrossRef]
- Kinney, W.H. Cosmology, Inflation, and the Physics of Nothing. *arXiv* **2003**, arXiv:astro-ph/0301448.
- Weinberg, S. *Cosmology*; Oxford University Press: Oxford, UK, 2008.
- Fixsen, D.J. The Temperature of the Cosmic Microwave Background. *Astrophys. J.* **2009**, *707*, 916. [CrossRef]
- Planck Collaboration. Planck 2018 results. VI. Cosmological parameters. *Astron. Astrophys.* **2020**, *641*, A6. [CrossRef]
- Friedmann, A. About the Curvature of Space. *J. Phys.* **1922**, *10*, 377.
- 't Hooft, G. The Inflationary Universe. *Nucl. Phys. B* **1974**, *79*, 276.
- Polyakov, A.M. Particle Spectrum in Quantum Field Theory. *JETP Lett.* **1974**, *20*, 194.
- Guth, A.H. The Inflationary Universe: A Possible Solution to the Horizon and Flatness Problems. *Phys. Rev. D* **1981**, *23*, 347. [CrossRef]
- Linde, A.D. A New Inflationary Universe Scenario: A Possible Solution of the Horizon, Flatness, Homogeneity, Isotropy and Primordial Monopole Problems. *Phys. Lett. B* **1982**, *108*, 389. [CrossRef]
- Linde, A.D. Inflationary Cosmology. *Lect. Notes Phys.* **2008**, *738*, 1.
- Linde, A.D. Chaotic Inflation. *Phys. Lett. B* **1983**, *129*, 177. [CrossRef]
- Odintsov, S.D. *et al.*, Recent Advances on Inflation. *Symmetry* **2023**, *10*, 1701. [CrossRef]
- Lyth, D.H. Particle physics models of inflation. *Lect. Notes Phys.* **2008**, *738*, 81.
- Riotto, A. Inflation and the Theory of Cosmological Perturbations. *arXiv* **2007**, arXiv:hep-ph/0210162.
- Kofman, L.; Linde, A.D.; Starobinsky, A.A. Towards the Theory of Reheating after Inflation. *Phys. Rev. D* **1997**, *56*, 3258. [CrossRef]
- Kolb, E.W. Dynamics of the Inflationary Era. *arXiv* **1999**, arXiv:hep-ph/9910311.
- Allahverdi, R.; Brandenberger, R.; Cyr-Racine, F.Y.; Mazumdar, A. Reheating in Inflationary Cosmology: Theory and Applications. *Ann. Rev. Nucl. Part. Sci.* **2010**, *60*, 27–51. [CrossRef]
- Linde, A.D. Inflationary Cosmology and Creation of Matter in the Universe. In *Modern Cosmology*; Bonometto, S., Gorini, V., Moschella, U., Eds.; Institute of Physics Publishing: Bristol, UK, 2002; pp. 159–185.
- Lozanov, K. Lectures on Reheating after Inflation. *arXiv* **2019**, arXiv:1907.04402.

27. Saha, P.; Anand, S.; Sriramkumar, L. Accounting for the Time Evolution of the Equation of State Parameter During Reheating. *Phys. Rev. D* **2020**, *102*, 103511. [[CrossRef](#)]
28. Weinberg, S. Effective Field Theory, Past and Future. *Int. J. Mod. Phys.* **2016**, *31*, 1630007. [[CrossRef](#)]
29. Lindblom, L. Causal Representations of Neutron-Star Equations of State. *Phys. Rev. D* **2018**, *97*, 123019. [[CrossRef](#)]
30. Ellis, G.F.R.; Maartens, R.; MacCallum, M.A.H. Causality and the Speed of Sound. *Gen. Rel. Grav.* **2007**, *39*, 1651. [[CrossRef](#)]
31. Thorne, K.S.; Blandford, R.D. *Modern Classical Physics*; Princeton University Press: Princeton, NJ, USA, 2017.
32. McLachlan, N.W. *Theory and Applications of Mathieu Functions*; Oxford University Press: London, UK, 1947.
33. Abramowitz, M.; Stegun, I. *Handbook of Mathematical Functions*; Dover: New York, NY, USA, 1972.
34. Birrell, N.D.; Davies, P.C.W. *Quantum Fields in Curved Space*; Cambridge University Press: Cambridge, UK, 1982.
35. Parker, L. The Creation of Particles by the Expanding Universe. Ph.D. Thesis, Harvard University, Cambridge, MA, USA, 1966.

**Disclaimer/Publisher's Note:** The statements, opinions and data contained in all publications are solely those of the individual author(s) and contributor(s) and not of MDPI and/or the editor(s). MDPI and/or the editor(s) disclaim responsibility for any injury to people or property resulting from any ideas, methods, instructions or products referred to in the content.